Journal of Biomolecular Structure and Dynamics

ISSN: 0739-1102 (Print) 1538-0254 (Online) Journal homepage: www.tandfonline.com/journals/tbsd20

Investigating the potential of novel thiazole derivatives in treating Alzheimer's and Parkinson's diseases

Abd Al Rahman Asfour, Asaf Evrim Evren, Begüm Nurpelin Sağlık Özkan & Leyla Yurttaş

To cite this article: Abd Al Rahman Asfour, Asaf Evrim Evren, Begüm Nurpelin Sağlık Özkan & Leyla Yurttaş (13 Dec 2024): Investigating the potential of novel thiazole derivatives in treating Alzheimer's and Parkinson's diseases, Journal of Biomolecular Structure and Dynamics, DOI: 10.1080/07391102.2024.2437521

To link to this article: https://doi.org/10.1080/07391102.2024.2437521

View supplementary material

Published online: 13 Dec 2024.

Submit your article to this journal

Article views: 218

View related articles

View Crossmark data

Full Terms & Conditions of access and use can be found at
https://www.tandfonline.com/action/journalInformation?journalCode=tbsd20

JOURNAL OF BIOMOLECULAR STRUCTURE AND DYNAMICS
https://doi.org/10.1080/07391102.2024.2437521

Taylor & Francis
Taylor & Francis Group

Check for updates

Investigating the potential of novel thiazole derivatives in treating Alzheimer's and Parkinson's diseases

Abd Al Rahman Asfour[a,b], Asaf Evrim Evren[a,c], Begüm Nurpelin Sağlık Özkan[a], and Leyla Yurttaş[a]

[a]Faculty of Pharmacy, Department of Pharmaceutical Chemistry, Anadolu University, Eskişehir, Turkey; [b]Institute of Graduate Education, Department of Pharmaceutical Chemistry, Anadolu University, Eskişehir, Turkey; [c]Department of Pharmacy Services, Bilecik Seyh Edebali University, Vocational School of Health Services, Bilecik

ABSTRACT

The study aimed to investigate 12 novel thiazole compounds in the treatment of neurodegenerative disorders. The compounds produced were evaluated for their inhibitory efficacy against acetylcholinesterase (AChE), butyrylcholinesterase (BChE), and monoamine oxidases (MAOs). Among the compounds, **5d**, **5e**, and **5j** showed the highest AChE inhibitory activity. The IC_{50} values for compounds are $0.223 \pm 0.010\ \mu M$, $0.092 \pm 0.003\ \mu M$, and $0.054 \pm 0.002\ \mu M$, respectively. In addition, molecular docking analyses and molecular dynamic simulation were used to examine the interactions of these compounds with protein sites. The results suggest that thiazole-ring compounds could serve as a promising basis for the development of drugs aimed at treating neurodegenerative diseases (NDD), caused by Parkinson's and Alzheimer's diseases.

ARTICLE HISTORY
Received 22 January 2024
Accepted 17 May 2024

KEYWORDS
Thiazole derivatives; neurodegenerative disorders; acetylcholinesterase inhibitors; molecular docking; molecular dynamic simulation studies

1. Introduction

Alzheimer's disease is a serious neurological disorder that leads to death and affects memory ability and other cognitive functions. Every year the number of people infected worldwide increases, making it a global health concern. This situation represents great difficulties for people and their families, as well as placing great pressure on healthcare systems and economies (Leoni et al., 2019; Mc.Conathy & Owens, 2003; Meng et al., 2015). Although the exact cause of Alzheimer's disease is not fully understood, several studies have identified some of the factors that contribute to the development of Alzheimer's disease, including S-protein buildup, beta-amyloid (Aβ) deposits, and mineral imbalances. AChE inhibitors increase acetylcholine levels in the brain, temporarily improving cognitive function. BChE inhibitors target another enzyme that breaks down acetylcholine (Hardy & Selkoe, 2002; Kalia & Lang, 2015; McKeith et al., 2017).

Parkinson's disease, a progressive neurological disorder, affects mobility and motor function. Parkinson's disease mostly affects substantia nigra dopaminergic neurons (Jankovic, 2008).

Although the exact cause of Parkinson's disease is unknown, it is believed to be a combination of genetic and environmental factors (Schapira et al., 2017). However, research has established that the depletion of biogenic monoamines and neurotransmitters such as dopamine, norepinephrine, and serotonin is an underlying factor in the pathological development of Parkinson's disease (Pålhagen et al., 2006). Monoamine oxidases (MAO) are enzyme proteins responsible for the degradation of these biogenic monoamines. There are two different types of monoamine oxidases MAO-A and MAO-B—which have different preferences for the substances they act on and the substances that might block their activity (Hirsch & Hunot, 2009; Iqbal et al., 2016; Prince et al., 2015). Research has shown that blocking the activity of MAO-B is successful in controlling NDDs such as Parkinson's and Alzheimer's disease. On the other hand, selectively inhibiting MAO-A has been proven to be beneficial in the treatment of anxiety and depression (Cummings, 2004; Heneka et al., 2015; Spires-Jones & Hyman, 2014).

Thiazole derivatives have shown promise as potential therapeutics for treating neurodegenerative disorders (Guo et al., 2013; Siezen & Galardini, 2008). These compounds have demonstrated the ability to interact with Aβ and modulate its aggregation process (Wang et al., 2017). By binding to Aβ, thiazole derivatives can disrupt the formation of harmful aggregates. This mechanism has the potential to reduce the accumulation of aggregates in the brain, thereby improving the condition of patients with Alzheimer's disease. Thiazole derivatives as MAO inhibitors have the potential to enhance dopaminergic neurotransmission and improve motor function in Parkinson's disease patients (Andreani et al., 1996; Huang & Yang, 2006; Hegab et al., 2008). They are also an essential pharmacophore and intermediate in producing agrochemicals and medicines. Thiazoles are present in various biologically active substances, including central nervous system (CNS) drugs such as Riluzole, Talipexole, and Pramipexole (Kumar et al., 1993). Thiazole analogues have also been discovered to have anti-diabetic, anti-glycation, and strong cholinesterase inhibitory properties, making them potential candidates for treating neurodegenerative

CONTACT Abd Al Rahman Asfour abdalrahmanasfour@anadolu.edu.tr, asfoor1994@gmail.com Faculty of Pharmacy, Department of Pharmaceutical Chemistry, Anadolu University, Eskişehir, Turkey.

Supplemental data for this article can be accessed online at https://doi.org/10.1080/07391102.2024.2437521.

© 2024 Informa UK Limited, trading as Taylor & Francis Group

disorders (Khan et al., 2015; Turan-Zitouni et al., 2013). On the other hand, the evolving understanding of the pharmacological mechanism of an acetanilide derivative, acetaminophene, reveals its neuroprotective properties owing to its anti-inflammatory and antioxidant properties, making it a subject of interest in the quest for developing small molecules against Alzheimer's and Parkinson's diseases (Tripathy & Grammas, 2009).

In view of these facts, this study aims to utilize a molecular hybridization approach to design and synthesize a library of new derivatives containing 2-aminothiazole and acetanilide moieties hoping to discover a new lead molecule as inhibitors of AChE, BChE, and MAO.

These novel thiazole compounds bearing acetanilide moiety were examined for their inhibitory activities against AChE, BChE, and MAO. Among them, compounds **5d**, **5e**, and **5j** demonstrated the highest inhibition of the enzyme AChE. However, their inhibition of BChE and MAO was relatively low. Docking analysis and Molecular Dynamic Simulation (MDS) techniques were conducted on the most active compounds **5d**, **5e,** and **5j** against AChE to understand their mechanism of enzyme inhibition. The study revealed strong interactions between the compounds and specific amino acids, primarily through hydrophilic, hydrophobic, hydrogen bonding, and π-π stacking interactions.

2. Materials and methods

2.1. Chemistry

All chemicals used were either from Merck [Merck KGaA, Darmstadt, Germany] or Sigma-Aldrich companies [Sigma Aldrich Corp., St. Louis, MO, USA]. The completion of the reactions of the compounds and their purity were confirmed using thin layer chromatography (TLC) manufactured on 60 F_{254} aluminum plates, as well as on silica gel supplied from Merck (Darmstadt, Germany). The melting points of the synthesized compounds were determined using the MP90 Digital Melting Point Instrument (Mettler Toledo, Ohio, USA) and were reported without any corrections. Infrared spectra results of the synthesized compounds were also obtained using Shimadzu-IR Affinity-IS equipment. The results of ^{1}H NMR and ^{13}C NMR spectra were also obtained using a Bruker 400 MHz and 100 MHz digital FT-NMR spectrometer (Bruker Bioscience, Billerica, MA, USA) in DMSO-d_6, respectively. The NMR spectra have several types of assigned splitting patterns, which are divided as follows: **s** for single, **d** for double, **t** for triple, and **m** for multiple. The constants (***J***) are given in Hertz. HRMS experiments were performed using an LC/MS-IT-TOF system manufactured by Shimadzu in Kyoto, Japan.

2.2. Synthesis of N-*(4-acetylphenyl) acetamide (1)*

In an ice bath, 4-aminoacetophenone (5 g, 0.036 mol), (1 equivalent), triethylamine (TEA) (1.5 equivalent), and tetrahydrofuran (THF) as a solvent (200 mL), were added to the reaction flask. Acetyl chloride (3.07 ml, 0.043 mol), (1.2 equivalent) was diluted with THF solvent in the dropping funnel and then dropped into the reaction flask for approximately three hours. Thin Layer Chromatography (TLC) was used to confirm that the reaction had ended, and then the mixture was poured into a glass dish. The solvent and TEA were evaporated under the fume hood, and distilled water was used to wash and filter the precipitated part, then left to dry.

2.3. N-*[4-(2-bromoacetyl) phenyl]acetamide (2)*

N-(4-acetylphenyl)acetamide (5.5 g, 0.031 mol) (1 equivalent) was added into a round flask with 1–2 drops of HBr, and acetic acid (200 mL) as solvent. Br_2 (1.91 mL, 0.037 mol) (1.2 equivalents) diluted with acetic acid in a drop funnel was dripped onto the round flask for approximately three hours. TLC has been used to confirm that the reaction had ended. After that, the product was added to ice water with continuous stirring and then filtered and left to dry.

2.4. N-*[4-(2-Aminothiazol-4-yl)phenyl]acetamide (3)*

N-[4-(2-Bromoacetyl)phenyl]acetamide (8.45 g, 0.033 mol) (1 equivalent) and thiourea (2.51 g, 0.033 mol) (1 equivalent) were added in a round flask with ethanol as a solvent (100 mL) and the reaction was boiled for about two hours under reflux. When the reaction was finished, the substance was poured into the beaker because of that the ethanol was permitted to evaporate under a fume hood, then the substance was scraped from the beaker and placed on the filter paper, washed with a little ethanol then left to dry.

2.5. N-*[4-(4-Acetamidophenyl) thiazol-2-yl]-2-chloropropanamide (4)*

N-(4-(2-Aminothiazol-4-yl)phenyl)acetamide (6.26 g, 0.027 mol) (1 equivalent), TEA (3.38 ml, 0.032 mol) (1.2 equivalent), and THF (200 mL) as solvent are mixed into the reaction flask and the reaction placed in an ice bath. 2-Chloropropionyl chloride (4.5 ml, 1.2 eq) was diluted with THF solvent in the dropping funnel and then dropped into the reaction flask for approximately three hours. TLC was used to confirm that the reaction had ended, then the mixture was poured into a glass dish, the solvent, and TEA were evaporated under the fume hood, and distilled water was used to wash and filter the precipitated part, then left to dry.

2.6. N-*[4-(4-Acetamidophenyl)thiazol-2-yl]-2-(heteroarylthio) propenamide (5)*

N-[4-(4-Acetamidophenyl)thiazol-2-yl]-2-chloropropanamide (0.25 g, 0.00077 mol) (1 equivalent), various heterocyclic mercaptan derivative (1 equivalent), and potassium carbonate (1 equivalent) in acetone (40 mL) solvent for one day at room temperature are mixed. TLC was used to confirm that the reaction had ended and then poured into the beaker to allow evaporation of the acetone under the fume hood. Distilled water was used to wash the compounds and they were dried. It was crystallized by ethanol.

2.6.1. N-[4-(4-Acetamidophenyl)thiazol-2-yl)-]2-((1-methyl-1H-imidazole-2 yl)thio)propanamide (5a)

Material appearance: powder, Color: pale yellow, Yield: 88%. M.P.:134 °C. IR (ATR) υ_{max} (cm^{-1}): 3174–3115 (N-H stretching) 2976–2929 (C-H stretching), 1668 (C = O stretching, amide), 1541–1408 (C = N stretching, and C = C stretching), 1062–1278 (C-N stretching).^{1}H-NMR (400 MHz, DMSO-d_6, ppm) δ: 1.44 (3H, d, J = 6.97 Hz, CH_3), 2.06 (3H, s, $COCH_3$), 3.59 (3H, s, N-CH_3), 4.15 (1H, q, J = 6.95 Hz, CH), 7.03 (1H, s, im-H_4), 7.34 (1H, s, im-H_5), 7.52 (1H, s, thiazole), 7.64 (2H, d, J = 8.52 Hz, Ph-$H_{2,6}$), 7.81 (2H, d, J = 8.54 Hz, Ph-$H_{3,5}$), 10.05 (1H, brs, $NHCOCH_3$), 12.59 (1H, brs, NH).^{13}C-NMR (100 MHz) (DMSO-d_6) δ (ppm): 17.66 ($CHCH_3$), 24.51($COCH_3$), 33.69 (NCH_3), 45.52 (CH), 107.51 (thi-C_5), 119.47 (Ph-$C_{3,5}$), 124.84 (Ph-$C_{2,6}$), 126.55 (Ph-C_1), 129.53 (im-$C_{4,5}$), 137.57 (Ph-C_4), 139.49 (Ph-C_4), 149.32 (im-C_2), 158.00 (thi-C_2), 168.80 ($COCH_3$), 170.52 (CO). HRMS (ESI) (m/z): $[M+1]^+$: Calculated for $C_{18}H_{19}N_5O_2S_2$: 401.1053; found: 401.1029.

2.6.2. N-[4-(4-Acetamidophenyl)thiazol-2-yl)-]2-[(1-methyl-1H-tetrazol-5-yl)thio]propanamide (5b)

Material appearance: powder, Color: pale yellow, Yield: 72%. M.P: 151 °C. IR (ATR) υ_{max} (cm^{-1}): 3304–3184 (N-H stretching), 3116–2978 (C-H stretching), 1668 (C = O stretching, amide), 1541–1408 (C = N stretching, and C = C stretching), 1267 (C-N stretching).^{1}H-NMR (400 MHz, DMSO-d_6, ppm) δ:1.63 (3H, d, J = 6.99 Hz, CH_3), 2.06 (3H, s, $COCH_3$), 3.97 (3H, s, N-CH_3), 4.60 (1H, q, J = 6.98 Hz, CH), 7.56 (1H, s, thiazole), 7.65 (2H, d, J = 8.21 Hz, Ph-$H_{2,6}$), 7.82 (2H, d, J = 8.21 Hz, Ph-$H_{3,5}$), 10.05 (1H, brs, $NHCOCH_3$), 12.68 (1H, brs, NH).^{13}C-NMR (100 MHz) (DMSO-d_6) δ (ppm): 18.72 ($CHCH_3$), 24.51($COCH_3$), 34.35(NCH_3), 46.22 (CH), 107.79 (thi-C_5), 119.48 (Ph-$C_{3,5}$), 126.57 (Ph-$C_{2,6}$), 129.43 (Ph-C_1), 139.52 (Ph-C_4), 149.42 (thi-C_4), 151.89 (tetrazole-C_5), 157.80 (thi-C_2), 168.81 ($COCH_3$), 169.51 (CO). HRMS (ESI) (m/z): $[M+1]^+$: Calculated for $C_{16}H_{17}N_7O_2S_2$ 404.0958.; found: 404.0950.

2.6.3. N-[4-(4-Acetamidophenyl)thiazol-2-yl)-]2-[(5-chlorobenzothiazol-2-yl)thio]propanamide (5c)

Material appearance: powder, Color: brown, Yield: 72%. M.P.: 180 °C. IR (ATR) υ_{max} (cm^{-1}): 3228–3180 (N-H stretching), 3084–2981 (C-H stretching), 1681 (C = O stretching, amide), 1597–1406 (C = N stretching, and C = C stretching), 1178–1010 (C-N stretching).^{1}H-NMR (400 MHz, DMSO-d_6, ppm) δ: 1.73 (3H, d, J = 6.94 Hz, CH_3), 2.08 (3H, s, $COCH_3$), 4.96 (1H, q, J = 6.94 Hz, CH), 7.44 (1H, d, J = 8.23 Hz, bt-H_6), 7.56 (1H, s, thiazole -H_5), 7.67 (2H, d, J = 8.33 Hz, Ph-$H_{2,6}$), 7.85 (2H, d, J = 8.39 Hz, Ph-$H_{3,5}$), 7.92 (1H, s, bt-H_4), 8.08 (1H, d, J = 8.57 Hz, bt-H_7), 10.07 (1H, s, $NHCOCH_3$), 12.81 (1H, s, NH).^{13}C-NMR (100 MHz) (DMSO-d_6) δ (ppm): 18.83 ($CHCH_3$), 24.51($COCH_3$), 46.62 (CH), 107.75 (thi-C_5), 119.49 (Ph-$C_{3,5}$), 121.22 (bt-C_4), 123.85 (bt-C_6), 125.28 (bt-C_7), 126.58 (Ph-$C_{2,6}$), 129.46 (ph-C_1), 131.78 (bt-C_5), 134.17 (bt-C_{7a}), 139.51 (ph-C_4), 149.41 (thi-C_4), 153.81 (bt-C_{3a}), 157.92 (thi-C_2), 167.59 (bt-C_2), 168.81 ($COCH_3$), 169.60 (CO). HRMS (ESI) (m/z): $[M+1]^+$: Calculated for $C_{21}H_{17}N_4O_2S_3Cl$: 489.0275; found: 489.0278.

2.6.4. N-[4-(4-Acetamidophenyl)thiazol-2-yl)-]2-[(5-methyl-1,3,4-thiadiazol-2-yl)thio]propanamide (5d)

Material appearance: powder, Color: light brown, Yield: 93%. M.P.: 140–143 °C. IR (ATR) υ_{max} (cm^{-1}): 3228–3180 (N-H stretching), 3084–2981 (C-H stretching), 1681 (C = O stretching, amide), 1597–1406 (C = N stretching, and C = C stretching), 1178–1010 (C-N stretching).^{1}H-NMR (400 MHz, DMSO-d_6, ppm) δ: 1.61 (3H, d, J = 6.98 Hz, CH_3CHCO), 2.07 (3H, s, $COCH_3$), 2.69 (3H, s, CH_3), 4.70 (1H, q, J = 6.96 Hz, CH), 7.54 (1H, s, thiazole-H_5), 7.65 (2H, d, J = 8.46 Hz, Ph-$H_{2,6}$), 7.83 (2H, d, J = 8.51 Hz, Ph-$H_{3,5}$), 10.04 (1H, s, $NHCOCH_3$), 12.68 (1H, s, NH).^{13}C-NMR (100 MHz) (DMSO-d_6) δ (ppm): 15.71 (CH_3CHCO), 18.41 (CH_3), 24.51 ($COCH_3$), 46.43 (CH), 107.69 (thi-C_5), 119.49 (Ph-$C_{3,5}$), 126.57 (Ph-$C_{2,6}$), 129.48 (Ph-C_1), 139.50 (Ph-C_4), 149.38 ($NCHCH_3$), 157.92 (thi-C_4), 162.41 (thiadiazole-C_2), 167.42 (thi-C_2), 168.81 ($COCH_3$), 169.72 (CO). HRMS (ESI) (m/z): $[M+1]^+$: Calculated for $C_{17}H_{17}N_5O_2S_3$: 420.0617; found 420.0613.

2.6.5. N-[4-(4-Acetamidophenyl)thiazol-2-yl]-2-[(5-nitro-1H-benzimidazol-2-yl)thio]propanamide (5e)

Material appearance: powder, Color: dark orange, Yield: 91%. M.P: 177 °C. IR (ATR) υ_{max} (cm^{-1}): 3080–3063 (N-H stretching), 2972–2931 (C-H stretching), 1681–1688 (C = O stretching, amide), 1405–1539 (C = N stretching, and C = C stretching), 1371 (N = O stretching), 1178–1008 (C-N stretching).^{1}H-NMR (400 MHz, DMSO-d_6, ppm) δ: 1.67 (3H, d, J = 7.03 Hz, CH_3), 2.07 (3H, s, $COCH_3$), 4.90 (1H, q, J = 7.00 Hz, CH), 7.52 (1H, s, thiazole-H_5), 7.58 (1H, d, J = 8.38 Hz, benzimidazole -H_7), 7.65 (2H, d, J = 8.38 Hz, Ph-$H_{2,6}$), 7.83 (2H, d, J = 8.41 Hz, Ph-$H_{3,5}$), 8.02 (1H, d, benzimidazole -H_6), 8.33 (1H, s, benzimidazole -H_4), 10.06 (1H, s, $NHCOCH_3$, NH).^{13}C-NMR (100 MHz) (DMSO-d_6) δ (ppm): 18.35 (CH_3), 24.50 ($COCH_3$), 44.13 (CH), 107.41 (thi-C_5), 110.89 (benzimidazole -C_7), 114.11 (benzimidazole -C_4), 117.11 (benzimidazole -C_5), 119.46 (Ph-$C_{3,5}$), 126.53 (Ph-$C_{2,6}$), 129.50 (Ph-C_1), 141.71 (Ph-C_4, benzimidazole -C_{7a}), 146.77 (benzimidazole -$C_{6,3a}$), 149.28 (benzimidazole -C_2), 158.01 (thi -C_4), 158.08 (thi -C_2), 168.80 ($COCH_3$), 170.61 (CO). HRMS (ESI) (m/z): $[M+1]^+$: Calculated for $C_{21}H_{18}N_6O_4S_2$: 483.0894; found 483.0904.

2.6.6. 2-[(1H-Benzimidazol-2-yl)thio]-N-[4-(4-acetamidophenyl)thiazol-2-yl]propanamide (5f)

Material appearance: powder, Color: pale yellow, Yield: 70%. M.P.: 149 °C. IR (ATR) υ_{max} (cm^{-1}): 3063 (N-H stretching), 2974–2961 (C-H stretching), 1668 (C = O stretching, amide), 1597–1406 (C = N stretching, and C = C stretching), 1094–1008 (C-N stretching). ^{1}H-NMR: (400 MHz, DMSO-d_6, ppm) δ: 1.66 (3H, d, J = 6.98 Hz, CH_3), 2.07 (3H, s, $COCH_3$), 4.83 (1H, q, J = 6.86 Hz, CH), 7.15 (2H, brs, benzimidazole-$H_{5,6}$), 7.51 (3H, brs, thiazole-H_5, benzimidazole-$H_{5,6}$), 7.66 (2H, d, J = 8.42 Hz, Ph-$H_{3,5}$), 7.83 (2H, d, J = 8.42 Hz, Ph-$H_{2,6}$), 10.09 (1H, s, NH). ^{13}C-NMR (100 MHz) (DMSO-d_6) δ (ppm): 18.86 (CH_3), 24.50($COCH_3$), 44.92 (CH), 107.41 (thi-C_5), 109.95 (benzimidazole-$C_{4,7}$), 119.48 (Ph-$C_{3,5}$), 122.12 (benzimidazole-$C_{5,6}$), 122.76 (), 126.53 (Ph-$C_{3,5}$), 129.61 (Ph-C_1), 132.71 (Ph-C_4), 139.42 (benzimidazole-C_2),149.07 (benzimidazole-C_{7a}), 149.25 (benzimidazole-C_{3a}), 158.59 (thi-C_4) 168,56

(thi-C_2),168.82 ($\underline{C}OCH_3$), 170,74 (CO). HRMS (ESI) (*m/z*): $[M+1]^+$: Calculated for $C_{21}H_{19}N_5O_2S_2$: 438.1053; found 438.1045.

2.6.7. N-[4-(4-Acetamidophenyl)thiazol-2-yl]-2-(benzothiazol-2-ylthio)propanamide (5 g)

Material appearance: powder, Color: light brown, Yield: 76%. M.P: 190 °C. IR (ATR) υ_{max} (cm^{-1}): 3244–3107 (N-H stretching), 3059 – 2988 (C-H stretching), 1687 (C = O stretching, amide), 1663–1423 (aromatic C = N stretching and C = C stretching), 1236–1002 (C-N stretching).^{1}H-NMR: (400 MHz, DMSO-d_6, ppm) *δ:* 1.71 (3H, d, *J* = 6.99 Hz, CH_3), 2.07 (3H, brs, $COCH_3$), 4.95 (1H, q, *J* = 7.03 Hz, CH), 7.39 (1H, t, *J* = 7.60 Hz, benzothiazole-H_5), 7.48 (1H, t, *J* = 7.67 Hz, benzothiazole-H_6), 7.55 (1H, s, thiazole-H_5), 7.65 (2H, d, *J* = 8.53 Hz, Ph-$H_{2,6}$), 7.84–7.87 (3H, m, *J* = 8.52 Hz, benzothiazole-H_4, Ph-$H_{3,5}$), 8.04 (1H, d, *J* = 7.95 Hz, benzothiazole-H_7). 10.05 (1H, s, $\underline{NH}COCH_3$). 12.78 (1H, s, NH).^{13}C-NMR (100 MHz) (DMSO-d_6) δ (ppm): 18.83 (CH_3), 24.52($\underline{C}OCH_3$), 46.47(CH), 107.73 (thiazole -C_5), 119.49 (Ph-$C_{3,5}$), 121.84 (benzothiazole-C_4), 122.44 (benzothiazole-C_7), 125.31(benzothiazole-C_6), 126.58 (Ph-$C_{2,6}$), 126.98 (benzothiazole-C_5), 129.48 (Ph-C_1), 135.41 (benzothiazole-C_{7a}), 139.50 (Ph-C_4), 149.39 (thiazole -C_4), 152.96 (benzothiazole-C_{3a}), 157.97 (thiazole -C_2), 164.66 (benzothiazole-C_9), 168.82 ($\underline{C}OCH_3$), 169.80 (CO). HRMS (ESI) (*m/z*): $[M+1]^+$: Calculated for $C_{21}H_{18}N_4O_2S_3$: 455.0665; found 455.0665.

2.6.8. N-[4-(4-Acetamidophenyl)thiazol-2-yl]-2-[(4-methyl-1H-1,2,4-triazol-3-yl)thio]propanamide (5h)

Material appearance: powder, Color: pale yellow, Yield: 81%. M.P: 201 °C. IR (ATR) υ_{max} (cm^{-1}): 3246–3176 (N-H stretching), 3115–2931 (C-H stretching), 1666 (C = O stretching, amide), 1566–1406 (C = N stretching, and C = C stretching), 1176–1060 (C-N stretching).^{1}H-NMR (400 MHz, DMSO-d_6, ppm) *δ:* 1.52 (3H, d, *J* = 6.83 Hz, $\underline{C}H_3CHCO$), 2.07 (3H, s, $COCH_3$), 3.58 (3H, s, CH_3), 4.31 (1H, q, *J* = 6.84 Hz, CH), 7.54 (1H, s, thiazole-H_5), 7.65 (2H, d, *J* = 8.05 Hz, Ph-$H_{2,6}$), 7.82 (2H, d, *J* = 7.96 Hz, Ph-$H_{3,5}$), 8.65 (1H, s, NCH), 10.05 (1H, s, $\underline{NH}COCH_3$), 12.57 (1H, s, NH).^{13}C-NMR (100 MHz) (DMSO-d_6) δ (ppm): 18.08 ($\underline{C}H_3CHCO$), 24.51($\underline{C}OCH_3$), 31.49 (CH_3), 45.32 (CH), 107.64 (thiazole-C_5), 119.48 (Ph-$C_{3,5}$), 126.56 (Ph-$C_{2,6}$), 129.48 (Ph-C_1), 139.48 (Ph-C_4), 147.00 (triazole-C_3), 147.20 (triazole-C_5), 149.38 (thiazole-C_4), 157.91 (thiazole-C_2), 168.82 ($\underline{C}OCH_3$), 170.07 (CO). HRMS (ESI) (*m/z*): $[M+1]^+$: Calculated for $C_{17}H_{18}N_6O_2S_2$: 403.1005; found 403.1008.

2.6.9. N-[4-(4-Acetamidophenyl)thiazol-2-yl]-2-(benzoxazol-2-ylthio)propanamide (5i)

Material appearance: powder, Color: brown, Yield: 85%. M.P.:159 °C. IR (ATR) υ_{max} (cm^{-1}): 3244–3180 (N-H stretching), 3107–2931 (C-H stretching), 1678–1660 (C = O stretching, amide), 1598–1406 (C = N stretching, and C = C stretching), 1236–1176 (C-N stretching).^{1}H-NMR (400 MHz, DMSO-d_6, ppm) *δ:* 1.74 (3H, d, *J* = 7.03 Hz, CH_3), 2.06 (3H, s, $COCH_3$), 4.88 (1H, q, *J* = 6.56 Hz, CH), 7.34 (2H, brs, *J* = 2.16 Hz, benzoxazole -$H_{4,7}$), 7.49 (1H, s, thiazole-H_5), 7.64 (4H, brs, *J* = 7.78 Hz, Ph-$H_{2,6}$, benzoxazole -$H_{5,6}$), 7.82 (2H, d, *J* = 8.40 Hz, Ph-$H_{3,5}$), 10.05 (1H, s, NH), ^{13}C-NMR (100 MHz) (DMSO-d_6) δ (ppm): 19.48 (CH_3), 24.50 ($\underline{C}OCH_3$), 46.89 (CH), 107.49 (thiazole -C_5), 110.76 (benzoxazole -C_4), 118.91(benzoxazole -C_7), 119.47 (Ph-$C_{3,5}$), 120.64 (benzoxazole -C_5), 122.16 (benzoxazole -C_6), 123.24 (Ph-C_1), 125.02 (Ph-C_4), 125.18 (benzoxazole -C_{7a}), 126.53 (Ph-$C_{2,6}$), 129.73 (thiazole -C_4), 139.39 (benzoxazole -C_{3a}), 141.64(thiazole -C_2), 149.26 (benzoxazole -C_2), 151.65($\underline{C}OCH_3$), 168.79(CO). HRMS (ESI) (*m/z*): $[M+1]^+$: Calculated for $C_{21}H_{18}N_4O_3S_2$: 439.0893; found 439.0891.

2.6.10. N-[4-(4-Acetamidophenyl)thiazol-2-yl]-2-[(5-chlorobenzoxazol-2-yl)thio]propanamide (5j)

Material appearance: powder, Color: brown, Yield: 98%. M.P.:165 °C. IR (ATR) υ_{max} (cm^{-1}): 3180–3115 (N-H stretching), 3066–2933 (C-H stretching), 1688 (C = O stretching, amide), 1597–1446 (C = N stretching, and C = C stretching), 1253–1060 (C-N stretching). ^{1}H-NMR (400 MHz, DMSO-d_6, ppm) *δ:* 1.75 (3H, d, *J* = 6.98 Hz, CH_3), 2.06 (3H, s, $COCH_3$), 4.93 (1H, q, *J* = 7.03 Hz, CH), 7.39 (1H, d, *J* = 8.66 Hz, benzoxazole-H_6), 7.56 (1H, s, thiazole-H_5,), 7.65 (2H, d, *J* = 8.24 Hz, Ph-$H_{2,6}$), 7.71 (1H, d, *J* = 8.66 Hz, benzoxazole -H_7), 7.82–7.84 (3H, m, *J* = 9.76 Hz, Ph-$H_{3,5}$, benzoxazole -H_4), 10.04 (1H, s, $\underline{NH}COCH_3$), 12.83 (1H, s, NH). ^{13}C-NMR (100 MHz) (DMSO-d_6) δ (ppm): 19.24 (CH_3), 24.51($\underline{C}OCH_3$), 46.28 (CH), 107.48 (thi-C_5), 112.09 (benzoxazole -C_4), 118.72 (benzoxazole -C_7), 119.48 (Ph-$C_{3,5}$), 125.04 (benzimidazole-C_5), 126.58 (Ph-$C_{3,5}$), 129.43 (Ph-C_1), 129.53 (benzoxazole-C_6), 139.52 (Ph-C_4),142.86 (benzoxazole-C_{7a}), 149.41 (benzoxazole-C_{3a}), 150.49 (thi-C_4) 157,85 (thi-C_2),165.00(benzoxazole-C_2), 168.81 ($\underline{C}OCH_3$), 169,42 (CO). HRMS (ESI) (*m/z*): $[M+1]^+$: Calculated for $C_{21}H_{17}N_4O_3S_2Cl$: 473.0503; found473.0503.

2.6.11. N-[4-(4-Acetamidophenyl)thiazol-2-yl]-2-(pyrimidin-2-ylthio)propanamide (5k)

Material appearance: powder, Color: light yellow, Yield: 74%. M.P.:153 °C. IR (ATR) υ_{max} (cm^{-1}): 3255 (N-H stretching), 3115 – 2976 (C-H stretching), 1681–1660 (C = O stretching, amide), 1597–1539 (C = N stretching, and C = C stretching), 1259–1060 (C-N stretching). ^{1}H-NMR (400 MHz, DMSO-d_6, ppm) *δ:* 1.59 (3H, d, *J* = 7.08 Hz, CH_3), 2.06 (3H, s, $COCH_3$), 4.77 (1H, q, *J* = 7.10 Hz, CH), 7.24 (1H, t, *J* = 4.88 Hz, pyrimidine-H_5), 7.52 (1H, s, thi-H_5), 7.64 (2H, d, *J* = 8.41 Hz, Ph-$H_{2,6}$), 7.82 (2H, d, *J* = 8.48 Hz, Ph-$H_{3,5}$), 8.65 (2H, d, *J* = 4.98 Hz, pyrimidine-$H_{4,6}$), 10.05 (1H, s, $\underline{NH}COCH_3$), 12.61 (1H, s, NH). ^{13}C-NMR (100 MHz) (DMSO-d_6) δ (ppm): 18.21 (CH_3), 24.51($COCH_3$), 43.70 (CH), 107.47 (thiazole-C_5), 118.11 (pyrimidine-C_5), 119.46 (Ph-$C_{3,5}$), 126.56 (Ph-$C_{2,6}$), 129.54 (Ph-C_1), 139.45 (Ph-C_4), 149.28 (thiazole-C_4), 158.20 (thiazole-C_2), 158.39 (pyrimidine-C_4), 159.03 (pyrimidine-C_6), 168.80 ($\underline{C}OCH_3$), 170.35 (CO), 170.84 (pyrimidine-C_5). HRMS (ESI) (*m/z*): $[M+1]^+$: Calculated for $C_{18}H_{17}N_5O_2S_2$: 400.0896; found 400.0896.

2.6.12. N-[4-(4-Acetamidophenyl)thiazol-2-yl]-2-[(5-methylbenzoxazol-2-yl)thio]propanamide (5 l)

Material appearance: powder, Color: pale yellow, Yield: 72%. M.P.:140 °C. IR (ATR) υ_{max} (cm^{-1}): 3292–3184 (N-H stretching), 3111–2978 (C-H stretching), 1688 (C = O stretching, amide), 1539–1408 (C = N stretching, and C = C stretching), 1257–1062 (C-N stretching). ^{1}H-NMR (400 MHz, DMSO-d_6, ppm) δ: 1.73 (3H, d, J = 6.95 Hz, CH_3CHCO), 2.07 (3H, s, $COCH_3$), 2.39 (3H, s, CH_3), 4.90 (1H, q, J = 6.91 Hz, CH), 7.14 (1H, d, J = 8.26 Hz, benzoxazole -$H_{6)}$, 7.46 (1H, s, thiazole-H_5), 7.53 (2H, t, J = 8.05 Hz, benzoxazole -$H_{4,7}$), 7.65 (2H, d, J = 8.26, Ph-$H_{2,6}$), 7.83 (2H, d, J = 8.37 Hz, Ph-$H_{3,5}$), 10.05 (1H, s, $NHCOCH_3$), 12.79 (1H, s, NH), ^{13}C-NMR (100 MHz) (DMSO-d_6) δ (ppm): 19.14 (CH_3CHCO), 21.35(CH_3), 24.51 ($COCH_3$), 45.97 (CH), 107.77 (thiazole-C_5), 110.16 (benzoxazole -C_4), 118.86 (benzoxazole -C_7), 119.49 (Ph-$C_{3,5}$), 125.92 (benzoxazole -C_5), 126.58 (Ph-$C_{2,6}$), 129.46 (Ph-C_1), 134.66 (benzoxazole -C_6), 139.52 (Ph-C_4), 141.78 (benzoxazole -C_{7a}), 149.41 (benzoxazole -C_{3a}), 149.95 (thiazole-C_4), 157.92 (thiazole-C_2), 162.77 (benzoxazole -C_2), 168.81 ($COCH_3$), 169.64 (CO). HRMS (ESI) (m/z): $[M+1]^+$: Calculated for $C_{22}H_{20}N_4O_3S_2$: 453.1050; found 453.1050.

2.7. ADME prediction

ADME prediction methods use both practical and computational techniques for evaluating the absorption, distribution, metabolism, and excretion characteristics of pharmaceutical compounds. In this study, the produced compounds were analyzed using the online SwissAdme tools (http://www.swissadme.ch) to estimate their physicochemical characteristics.

2.8. Biological activity

2.8.1. Determination of AChE and BChE inhibition

By dissolving the AChE and BChE enzymes in water, a 1% gelatin solution was created. The enzymes were dissolved in gelatine solution to reach a 500 U/mL concentration. To make a 5 U/mL stock solution, 100 mL of H_2O was combined with one mL of the enzyme solution in a measuring flask, subsequently split into 0.7 mL parts, and kept at −20 °C. The portions of enzyme solution were thawed and allowed to reach room temperature before use. Each aliquot was then diluted with water to a concentration of 2.5 U/mL by filling the 0.7 mL container to 1.4 mL with water.

2.8.2. AChE enzyme kinetics study

The experimental protocol for the kinetic studies was exactly the same as that of the inhibition study. However, unlike the inhibition method, the selected compound was used at the calculated concentrations of $2 \times IC_{50}$, IC_{50}, and $IC_{50}/2$. For AChE enzymes, the substrate (acetylthiocholine iodide (ATC)) solution was used with serial dilutions at 6 different concentrations (600, 300, 150, 75, 37.5, and 18.75 μM). The measurements were carried out separately with and without an inhibitor. Obtained absorbance values were analyzed against varying substrate concentrations in the Microsoft Office Excel-2013 software and Lineweaver-Burk plots were drawn (Ceyhun et al., 2022; Hussein et al., 2018; Osmaniye et al., 2022; Sağlık et al., 2016; Tok et al., 2019; Yamali et al., 2021).

2.8.3. Determination of MAO inhibition

An *in vitro* fluorometric approach was used to evaluate the potential of the produced compounds in inhibiting MAO isoenzymes. Tyramine (200 L, 100 mM), Ampliflu™ Red (200 μL, 20 mM), and horseradish peroxidase (200 U/mL, 100 μL) were dissolved in in PO_4^{3-} buffer as part of the method. Additionally, newly made solutions of resurfacing *h*MAO-B (0.64 U/mL) and *h*MAOA (0.5 U/mL) enzymes in phosphate buffer and inhibitors in 2% DMSO (10^{-3}–10^{-9} M) were made. The calibrated total solution volume was 10 mL (Evren et al., 2022).

The experiment began by combining *h*MAO-A or *h*MAO-B enzyme solutions and inhibitor solutions (20 μL/well) on a 96-well micro test plate. The plate was then incubated at 37 °C for 30 min. After that, the working solution (100 μL/well) was added, and the plate was incubated for another 30 min. The fluorescence of the plate was measured at 5-min intervals using Ex/Em = 535/587 nm to quantify the fluorescence. To determine the inhibitory effect of the produced compounds on horseradish peroxidase, the fluorescence of the plate was measured when a 3% H_2O_2 solution (20 mM, 100 μL/well) was used instead of enzyme solutions. Furthermore, the combination of inhibitor and working solutions was used to assess the non-enzymatic inhibition of the compounds (Osmaniye et al., 2022; Sağlık et al., 2019).

The equation was used to calculate the percent inhibition, and each experiment was repeated four times. All research was done in quadruplicate, and the equation was used to calculate the percent inhibition (1),

$$\%\ \text{inhibition} = \frac{[(FCt2 - FCt1) - (Fit2 - Fit1)]}{FCt2 - FCt1} * 100 \qquad (1)$$

The fluorescence found in a control well at time t2 is referred to as FCt2, while the fluorescence seen in the same well at time t1 is referred to as FCt1. The fluorescence recorded in an inhibitor well at time t2 is referred to as FIt2, while the fluorescence detected in the same well at time t1 is referred to as FIt1.

2.9. In silico methods

2.9.1. ADME prediction

ADME prediction methods use both practical and computational techniques for evaluating the absorption, distribution, metabolism, and excretion characteristics of pharmaceutical compounds. In this study, the produced compounds were analyzed using the online SwissAdme tools (http://www.swissadme.ch) to estimate their physicochemical characteristics.

2.9.2. Molecular modeling studies

All molecular Docking studies were carried out using Schrödinger (v2021-1, Schrödinger, Inc., New York, USA) with a Maestro interface.

2.9.2.1 Preparation of 4EY7 protein. The AChE protein structure (4EY7) was obtained from the Protein Data Bank (www.pdb.org, accessed March 18, 2023) in "PDB" format for computational investigations. The structure was refined using Maestro's Protein Preparation Wizard, which included the removal of crystals and water molecules. To speed up the computations, the attention was exclusively focused on chain A and its constituents, while disregarding chain B and any constituents inside such as solvents and other heteroatoms. The preparation process included completing the gaps in loops and side chains, introducing hydrogens, and minimizing using the OPLS4 force field.

2.9.2.2 Ligand preparation. The three-dimensional (3D) structures of the ligands were constructed using the Builder module in Maestro. Subsequently, the ligands were prepared using the LigPrep module of Maestro (v2021-1, Schrodinger, Inc., New York). No tautomers were generated and all the ligands were subjected to energy minimization using the OPLS4 force (Trawally et al., 2024; Yücel et al., 2024).

2.9.2.3 Molecular docking. To define the active pocket of the enzyme, a receptor grid box was generated by selecting the centroid of the co-crystallized ligand using the Grid Generation module. Ligands with a length of $\leq$ 20 Å were allowed to dock. Using the generated grid, docking studies were conducted with Schrodinger's Glide ligand docking program. As conducted by previous studies, standard precision mode (SP) and flexible ligand sampling were applied with the rest of the parameters maintained as default (Al-Sharabi et al., 2023; Osmaniye et al., 2022; Trawally et al., 2022; Yücel et al., 2024).

2.9.2.4 Molecular dynamic simulation studies. MDS was used to assess the binding interactions and time-dependent stability of a ligand-target complex. To conduct the simulations as performed in our previous studies (Çevik et al., 2022; Durmaz et al., 2022; Osmaniye et al., 2022, 2023; Turan Yücel et al., 2022), the Desmond program was utilized. which employed the Schrödinger Suite with a TIP3P water model for system builder, and orthorhombic box shape was assigned with distances 10, followed by a system neutralization using Na^+ and Cl^- ions. The system was subsequently energy minimized using the standard OPLS3e force field (Çevik et al., 2022; Durmaz et al., 2022; Osmaniye et al., 2022, 2023; Turan Yücel et al., 2022). The equilibration of the system was performed with the default protocol provided in Desmond, which consists of a series of restrained minimizations and molecular dynamics simulations used to slowly relax the system. The system was finally simulated for 100 ns using the NPT ensemble at constant temperature (310.55 K, Nose-Hoover Chain, default values) and pressure (1 bar, Martyna-Tobias-Klein, default values) utilizing the RESPA integrator to integrate the equations of motion. The cutoff for van der Waals and short-range electrostatic interactions was set at 9.0 Å. After performing MDS, the obtained trajectories were analyzed, and the values for the radius of gyration (Rg) (Luo et al., 2015; Zhao et al., 2022), root mean square deviation (RMSD), and root means square fluctuation (RMSF) were calculated (Wang et al., 2022).

3. Results and discussion

3.1. Chemistry

The compounds were synthesized in the laboratory through a five-step process (Scheme 1). Firstly, the compound 4-aminoacetophenone was reacted with acetyl chloride in the presence of triethylamine and THF nonpolar aprotic solvent to introduce the acetyl group, forming *N*-(4-acetylphenyl) acetamide. In the second step, *N*-(4-acetylphenyl)acetamide was reacted with bromine in acetic acid solvent with droplets of hydrobromic acid to form *N*-[4-(2-bromoacetyl)phenyl]acetamide. The third step involved the closure of the thiazole ring *via* a Hantzsch synthesis reaction between *N*-[4-(2-bromoacetyl)phenyl]acetamide and thiourea in ethanol solvent with heat. In the fourth step, a second acetyl group was added to *N*-[4-(2-aminothiazol-4-yl)phenyl]acetamide by reacting with 2-chloropropionyl chloride in the presence of triethylamine and tetrahydrofuran solvent. The final product was *N*-[4-(4-acetamidophenyl)thiazol-2-yl]-2-chloropropanamide.

In the last step, all 12 compounds were synthesized by reacting the mercaptan-heterocyclic rings (Table 1) with *N*-[4-(4-acetamidophenyl)thiazol-2-yl]-2-chloropropanamide in the presence of potassium carbonate as a catalyst and acetone as a solvent. This one-day reaction resulted in yields ranging from 70 to 98% for the final compounds **5a–5l**. The purity and chemical structure of all synthesized compounds were

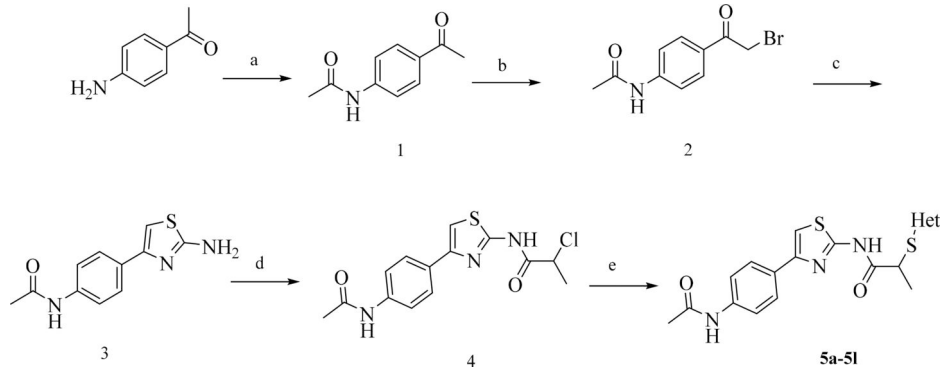

Scheme 1. Synthesis of the compounds (**5a–5l**). Reactants/reagents and reaction conditions. a: TEA, THF, 0–5 °C, then r.t., 3h; b: Br_2, HBr, AcOH; c: Thiourea, EtOH, 2h, reflux; d: 2-Chloropropionyl chloride, TEA, THF, 0–5 °C; e: Mercaptan derivatives, K_2CO_3, overnight, acetone, r.t.

Table 1. Heterocyclic rings for all synthesized compounds.

Compound	Heterocyclic	Compound	Heterocyclic
5a	1-methyl-1*H*-imidazol-2-yl	**5g**	Benzothiazol-2-yl
5b	1-methyl-1*H*-tetrazol-5-yl	**5h**	4-methyl-4*H*-1,2,4-triazol-2-yl
5c	5-chlorobenzothiazol-2-yl	**5i**	Benzoxazol-2-yl
5d	5-methyl-1,3,4-thiadiazol-2-yl	**5j**	5-chlorobenzoxazol-2-yl
5e	5-nitro-1*H*-benzimidazol-2-yl	**5k**	pyrimidin-2-yl
5f	1*H*-benzimidazol-2-yl	**5 l**	5-methylbenzoxazol-2-yl

Table 2. The study focuses on determining how the active compounds **5d, 5e,** and **5j** are processed by the body, including how they are absorbed, distributed, metabolized, and eliminated.

Compounds	M.W.	TPSA	Log Po/w (XLOGP3)	Log S (ESOL)	(LogKp) cm/s[11]	Lipinski	GI abs	HA	HD
5d	419.54	178.65	3.12	−4.32	−6.64	Yes	low	5	2
5e	482.54	199.13	3.67	−5	−6.64	Yes	low	6	3
5j	472.97	150.66	4.74	−5.71	−5.82	Yes	low	5	2
S1	379.49	38.77	4.28	−4.81	−5.58	Yes	High	4	0
S2	268.74	41.57	1.49	−2.36	−6.88	Yes	High	3	1

MW (molecular weight), TPSA (the topological polar surface area), Log P (partition coefficient), LogKp: skin permeation, Log S: aqueous solubility (highly soluble > 0 > very soluble > −2 > soluble > −4 > moderately soluble > −6 > poorly soluble > −10 > insoluble), GI abs (gastrointestinal absorption), HA (Hydrogen bond acceptor), HD (Hydrogen bond donor). S1: Donepezil; S2: Moclobemide.

confirmed using various chemical spectral analysis techniques such as IR, ^{1}H-NMR, ^{13}CNMR, and HRMS. All synthesized compounds are original derivatives.

Compounds (**5a–5l**) were analyzed by IR to determine their functional groups. The N-H group had a band above 3000 cm^{-1} (3063–3292 cm^{-1}). The C-H aromatic of sp^2 hybridized carbons had a value above 3000 cm^{-1}, except for **5g** (2974 cm^{-1}), while the aliphatic C-H of sp^3 hybridized carbons were observed below 3000 cm^{-1} (2848–2988 cm^{-1}). The (C = O) group had a band around 1688 cm^{-1} (1660–1688 cm^{-1}). The (C = N) group had a value between 1537 and 1597 cm^{-1}, except for **5g** (1663 cm^{-1}). The (C = C) aromatic group of sp^2 hybridized carbons recorded a band ranging from 1405 to 1489 cm^{-1}, except for **5k** (1539 cm^{-1}), while the (C-N) group was observed between 1002 and 1267 cm^{-1}.

Compounds with a thiazole ring bound to *N*-phenylacetamide at the 4th position were synthesized. NMR analysis was performed using a Bruker UltraShield 400 MHz spectrometer with samples dissolved in DMSO-d_6. A quintet at 2.5 ppm and a singlet at approximately 3.4 ppm indicating the presence of water protons were observed in all spectra. In the aliphatic region, three carbons containing protons were found in all compounds with values ranging from 1.44–1.75 ppm (doublet CH_3), 2.08–2.51 ppm (singlet $COCH_3$), and 4.15–4.96 ppm (quartet CH). Compounds **5a, 5b, 5d, 5h,** and **5 l** had singlet aliphatic protons branched from the azo group of the rings. In the aromatic region, the values of proton peaks varied in different compounds. The peaks belonging to C_4 and C_5 protons in the imidazole ring of **5a** appeared as a singlet, while the C_6 and C_7 protons of the benzothiazole group in **5c** appeared as a doublet. Compound **5f** showed unexpected singlet peaks for all protons of the carbons ring. The protons of the phenyl ring were seen as doublet peaks, and the thiazole ring had a singlet peak belonging to position C_5-H. The protons of the two amide groups sometimes appeared as a singlet between 10.03 and 12.83 ppm and sometimes did not appear due to the link with the nitrogen atom.

^{13}C-NMR analysis was performed using a Bruker UltraShield instrument with DMSO-d_6 as the solvent. The thiazole ring had peaks of C_2, C_4, and C_5 in all compounds between 107.79 and 168.56 ppm, with C_2 most deshielded. All aromatic carbons in all compounds showed peaks between about 110–162 ppm. The carbonyl carbon exhibited the greatest degree of deshielding, with a range of 168.79–170.74 ppm. The carbonyl attached to CH_3 was deshielded to a degree of 151.65–168.82 ppm. The solvent peak was detected as a septet with a chemical shift of approximately 40 ppm, and the analysis of each sample took 60 min.

The LCMS-IT-TOF was used to analyze the mass spectra of all the synthesized compounds. This technique involved injecting the samples through liquid chromatography before analyzing their mass using a mass spectrometer unit. The mass spectra of all the final compounds were taken using a high-resolution mass-spectrometry device with the ESI method. The obtained results indicated that there were no impurities in the chromatogram, and the $[M+1]$ peaks in the mass spectra of all the compounds correspond to their expected molecular weights (Glish & Vachet, 2003).

3.2. ADME parameters

Table 2 presents the expected pharmacokinetic characteristics of compounds **5d, 5e,** and **5j,** as well as the reference drugs Moclobemide and Donepezil. The SwissADME website was used to predict the pharmacokinetic characteristics of the most effective compounds. The topological polar surface area (TPSA) values for the compounds were high, ranging from 150.66 to 199.13 Å^2. The LogPo/w values were within the required range of −0.7 to 5, indicating appropriate lipophilicity (Daina et al., 2017). The compounds were found to have medium aqueous solubility, except for Moclobemide, which was soluble. The compounds exhibited low gastrointestinal absorption, which is a limitation. The number of hydrogen-bond acceptors varied among the compounds, with **5e** showing the highest value. The compounds also had varying numbers of hydrogen bond donors.

Table 3. Inhibition rates and IC50 (μM) values of the obtained compounds against AChE and BChE enzymes at concentrations of 10^{-3} and 10^{-4} M.

	AChE % inhibition			BChE % inhibition		
Compound	10^{-3} M	10^{-4} M	$AChEIC_{50}$ (μM)	10^{-3} M	10^{-4} M	$BChEIC_{50}$ (μM)
5a	52.323 ± 1.122	42.597 ± 1.454	>100	26.462 ± 0.834	22.746 ± 0.720	>1000
5b	48.154 ± 0.936	41.357 ± 1.010	>1000	29.375 ± 0.920	26.128 ± 0.967	>1000
5c	42.759 ± 0.806	38.964 ± 0.821	>1000	30.613 ± 1.258	26.408 ± 0.857	>1000
5d	89.646 ± 1.958	83.342 ± 1.768	0.223 ± 0.010	31.045 ± 1.041	24.067 ± 0.812	>1000
5e	92.155 ± 1.874	88.464 ± 1.334	0.092 ± 0.003	24.246 ± 0.865	20.771 ± 0.830	>1000
5f	72.849 ± 2.485	48.328 ± 0.889	>100	32.749 ± 1.059	26.697 ± 0.718	>1000
5g	47.764 ± 1.030	31.146 ± 1.302	>1000	30.569 ± 1.156	20.203 ± 0.801	>1000
5h	43.233 ± 0.955	29.031 ± 0.847	>1000	27.322 ± 0.948	22.345 ± 0.720	>1000
5i	57.954 ± 1.537	30.897 ± 0.867	>100	28.048 ± 0.864	21.470 ± 0.869	>1000
5j	93.576 ± 2.846	90.655 ± 1.920	0.054 ± 0.002	26.468 ± 0.854	23.876 ± 0.778	>1000
5k	74.290 ± 2.110	47.231 ± 0.886	>100	29.567 ± 0.975	25.661 ± 0.897	>1000
5l	69.067 ± 1.854	38.468 ± 0.736	>100	28.357 ± 0.923	22.554 ± 0.764	>1000
Donepezil	99.156 ± 1.302	97.395 ± 1.255	0.0201 ± 0.0010	–	–	–
Tacrine	–	–	–	99.827 ± 1.378	98.675 ± 1.450	0.0064 ± 0.0002

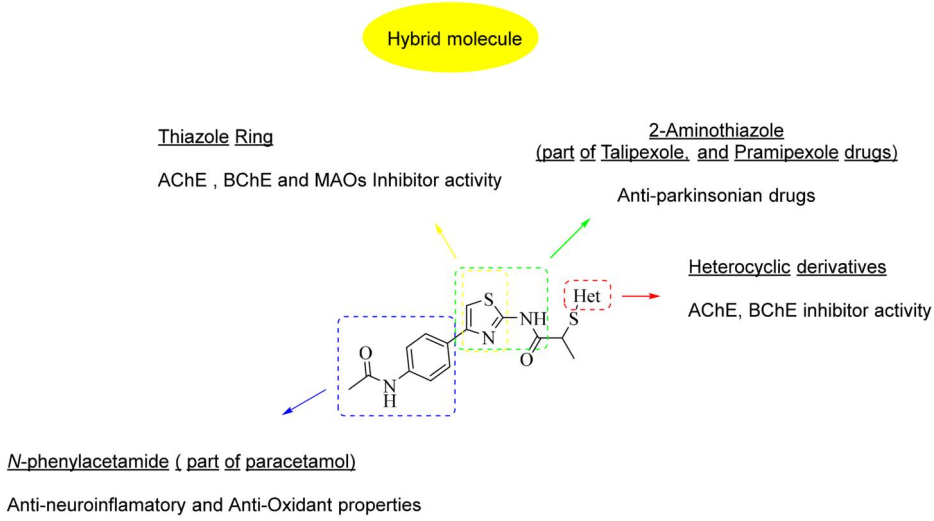

Figure 1. Rational design of compounds **5a–5l**.

3.3. Biological activity results

3.3.1. In vitro *anticholinesterase inhibition results evaluation*

Synthesized compounds were tested *in vitro* for their inhibitory effects on AChE and BChE. The compounds were more effective as AChE inhibitors. Elman's modified method was used to determine the percentage of inhibition with concentrations of 10^{-3} M and 10^{-4} M (Bourne et al., 1995). Compounds that showed over 50% inhibition were further tested at lower concentrations to determine their IC_{50} values (Table 3). Among them, compounds **5d, 5e**, and **5j** were selected for IC_{50} determination against AChE. The IC_{50} values for **5d, 5e,** and **5j** were 0.223, 0.092, and 0.054 μM, respectively. Compound **5j** was found to be the most effective with an IC_{50} of 0.054 μM. The presence of a benzoxazole group with chlorine at position 5 of the ring bonded with sulfur was found to be important for effectiveness. However, replacing the chlorine atom with a methyl group reduced the effectiveness significantly. The benzoxazole ring was also found to be important for effectiveness and replacing it with certain other rings decreased effectiveness (Figure 1). Unfortunately, all compounds showed low efficacy against BChE below 50% with notable IC_{50} values.

3.3.2. Enzyme kinetics on AChE

As mentioned in the enzyme inhibition assay compound **5j** was found to be the most effective agent on AChE enzyme. Enzyme kinetics studies were carried out to evaluate this compound's inhibition nature. The Lineweaver-Burk graphic was plotted using the absorbance values obtained in the tests and substrate concentrations. The graphics include four lines for enzyme kinetic tests applied to $2xIC_{50}$, IC_{50}, and $IC_{50}/2$ concentrations of the test compounds, and to the control group, that is, without inhibitor. The type of the reaction of substrate and inhibitor against the enzyme is determined according to the intersection of these four lines on the graphic.

Enzyme inhibition is typically divided into two categories reversible and irreversible. In irreversible inhibition, the inhibitor binds to an enzyme either covalently or forms a recalcitrant complex structure. The reversible inhibition category is also divided into four types: mixed type, competitive, noncompetitive, and uncompetitive inhibition types. The type of inhibition at Lineweaver-Burk graphics is defined as uncompetitive if four lines are parallel, competitive if the lines intersect on axis y, noncompetitive if the lines intersect on axis x, and mixed if four lines within the areas of the graphic but out of any axis (Ceyhun et al., 2022; Hussein

et al., 2018; Osmaniye et al., 2022; Sağlık et al., 2016; Tok et al., 2019; Yamali et al., 2021). As seen in the Lineweaver-Burk plot of compound **5j** (Figure 2), four lines intersect in the area outside the axes. This observation indicated that compound **5j** was a reversible and mixed-type inhibition with similar inhibition features as the substrates. The K_i value of compound **5j** was calculated as 0.0957 μM with the help of a secondary plot.

3.3.3. Evaluation of In vitro MAO inhibition results

The effectiveness of all compounds against both MAO-A and MAO-B enzymes showed similar results (Table 4). The percentage inhibition for MAO-A compounds ranged between 25.362 and 38.461% for a concentration of 10^{-3}, and between 20.415 and 31.748% for a concentration of 10^{-4}. On the other hand, for MAO-B, the inhibition percentage ranged between 30.886 and 45.441% for a concentration of 10^{-3}, and between 23.447 and 32.712% for a concentration of 10^{-4}. Although some compounds showed greater efficacy against MAO-B than MAO-A, all values were considered weak compared to Moclobemide and Selegiline.

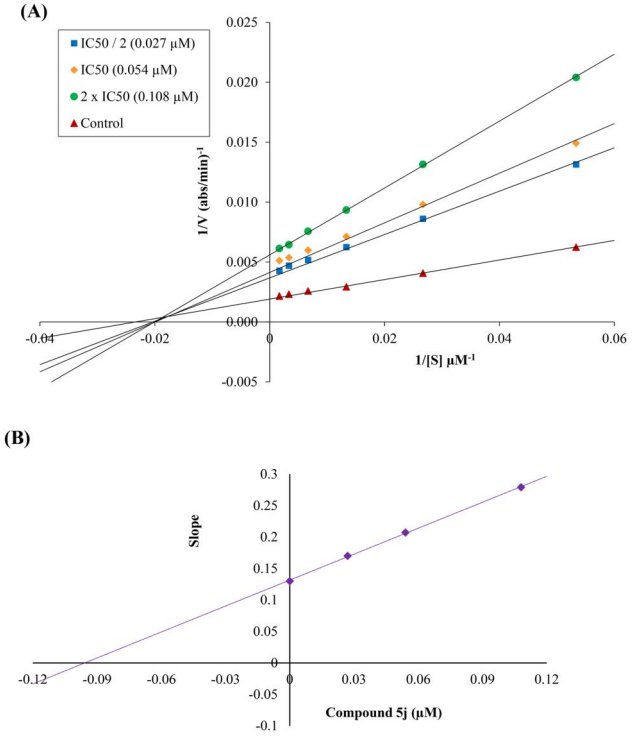

Figure 2. (A) Lineweaver-Burk plots for the inhibition of AChE by compound **5j**. [S], substrate concentration (μM); V, reaction velocity (nmol/min/mg protein). Inhibitor concentrations are shown on the left. (B) Secondary plot (Dixon plot) for the calculation of the steady-state inhibition constant (K_i) of compound **5j**. K_i was calculated as 0.0957 μM.

3.2.1. Structure–activity relationship evaluation

Based on the outcomes of both effectiveness and computational studies conducted on AChE, the compounds exhibited distinct SAR patterns, as outlined below.

The thiazole ring and benzene ring share many hydrophobic bonds that are formed by π–π stacking overlapping bonds. It contributes to the stability of the ligand within the protein, and the thiazole ring has a key role in inhibiting the AChE enzyme. Also, the two amide groups in the compound showed great importance in the stability of the compound, as the oxygen atom made hydrophilic bonds with amino acids, also the stability of the compound led to good results in terms of effectiveness. In the R groups, we have placed several rings such as benzoxazole, triazole, tetrazole, benzimidazole, thiadiazole, benzothiazole, and pyrimidine. The study found that benzoxazole rings were more effective than benzothiazole and thiadiazole rings, all of them formed π–π stacking bonds with amino acids. The majority of bonds with benzoxazole contain four bonds and this indicates its importance in stability three bonds with benzothiazole and two with thiadiazole. The chlorine atom at the 5th position of the benzoxazole ring was found to be crucial for its effectiveness. Removing this chlorine atom in compound **5i** reduced its effectiveness. Replacing the chlorine atom with a methyl group in compound **5l** resulted in a significant reduction in effectiveness which means the Cl atom makes an important activity. While the benzoxazole ring was found to be important for effectiveness, replacing it with certain other rings could also result in effectiveness. For example, compounds **5d** and **5e**, which replaced the benzoxazole ring with (2-methyl-1,3,4-thiadiazole) and (5-nitro-1*H*-benzimidazole), respectively. However, replacing the benzoxazole ring with other rings such as tetrazole, benzothiazole, triazole, and pyrimidine led to a decrease in effectiveness (Figure 3).

Table 4. Inhibition rates and IC_{50} (μM) values of the obtained compounds against MAO-A and MAO-B enzymes at concentrations of 10^{-3} and 10^{-4} M.

	MAO-A % Inhibition			MAO-B % Inhibition		
Compound	10^{-3} M	10^{-4} M	MAO-AIC_{50} (μM)	10^{-3} M	10^{-4} M	MAO-BIC_{50} (μM)
5a	32.521 ± 0.830	26.384 ± 0.820	>1000	42.449 ± 0.934	32.174 ± 0.747	>1000
5b	36.403 ± 1.176	29.636 ± 0.915	>1000	39.534 ± 1.225	31.050 ± 1.039	>1000
5c	30.791 ± 1.068	20.415 ± 0.944	>1000	45.441 ± 0.984	28.623 ± 1.018	>1000
5d	37.964 ± 1.151	21.152 ± 0.785	>1000	42.822 ± 1.562	32.712 ± 0.933	>1000
5e	29.554 ± 0.820	22.167 ± 0.935	>1000	38.774 ± 1.467	31.955 ± 1.202	>1000
5f	33.362 ± 1.348	28.530 ± 0.720	>1000	36.451 ± 1.208	29.574 ± 1.055	>1000
5g	38.461 ± 0.922	29.654 ± 0.964	>1000	39.113 ± 1.235	29.494 ± 0.957	>1000
5h	32.007 ± 0.828	30.067 ± 0.939	>1000	41.464 ± 0.837	31.646 ± 1.062	>1000
5i	36.867 ± 1.351	31.748 ± 1.120	>1000	35.774 ± 1.348	30.722 ± 1.168	>1000
5j	30.484 ± 0.989	24.425 ± 0.737	>1000	36.959 ± 1.534	32.536 ± 0.920	>1000
5k	25.362 ± 0.866	21.168 ± 1.011	>1000	30.886 ± 1.467	23.447 ± 0.958	>1000
5l	38.155 ± 1.476	33.831 ± 1.317	>1000	32.303 ± 0.918	24.628 ± 0.851	>1000
Moclobemide	94.121 ± 2.760	82.143 ± 2.691	6.0613 ± 0.2625	–	–	–
Selegiline	–	–	–	98.589 ± 2.055	94.850 ± 1.114	0.0374 ± 0.0016

3.4. Molecular docking studies

The active site of AChE is a narrow and deep gorge that contains amino acid residues responsible for catalysis and substrate binding. The binding site of AChE involves various amino acid residues, such as tryptophan, tyrosine, histidine, serine, glycine, and glutamate. Tryptophan and tyrosine residues interact with the ligand *via* hydrophobic interactions, while histidine, serine, and glutamate residues form hydrogen bonds with the ligand. Additionally, glycine residues contribute to the flexibility of the active site, allowing it to adjust to the shape of the ligand (Harel et al., 1993; Kenyon et al., 1991; Millard et al., 1999; Shintani et al., 2006).

The binding sites within AChE can be classified into two types: the central catalytic anionic site (CAS) and the peripheral anionic site (PAS). Both sites are involved in the regulation of AChE activity and have been the subject of extensive research (Shintani et al., 2006).

The CAS is a narrow, hydrophobic gorge that includes the acyl binding site, the active center, the hydrophobic subsite, the oxyanion binding site, and a catalytic triad of amino acids responsible for the hydrolysis of acetylcholine (Bourne et al., 1995; Martorana et al., 2016). The PAS is mainly composed of aromatic residues that provide a binding site for allosteric inhibitors and play a crucial role in regulating the activity of AChE by modulating the enzyme allosterically (Greenblatt et al., 1999). Docking studies have been used to predict the binding mode of ligands to both the CAS and the PAS of AChE in comparison with the previous studies (Al-Sharabi et al., 2023; Osmaniye et al., 2022; Sağlık et al., 2022), and some compounds have been identified that effectively bind to the active site and inhibit AChE activity (Harel et al., 1993). Thus, we have performed docking studies on compounds **5d**, **5e**, and **5j** and subsequent MD simulations on the most potent compound, **5j**, to analyze their interactions with AChE. Table 5 summarizes binding interactions of the compounds. This work diverged from the conventional use of verified docking for evaluating genomic databanks (Daoud & Taha, 2020; Lokwani et al., 2020; Maryam et al., 2021). Alternatively, this study used a docking approach that included experimental activity outcomes. Therefore, efforts were made to determine the most effective and significant binding position for the active compounds, in order to understand their binding methods as described in earlier studies (Abbas et al., 2017; Evren et al., 2023; Turan Yücel et al., 2022; Yücel et al., 2021). A three-dimensional image in Figure 4 displays the most effective compounds that are linked to the protein.

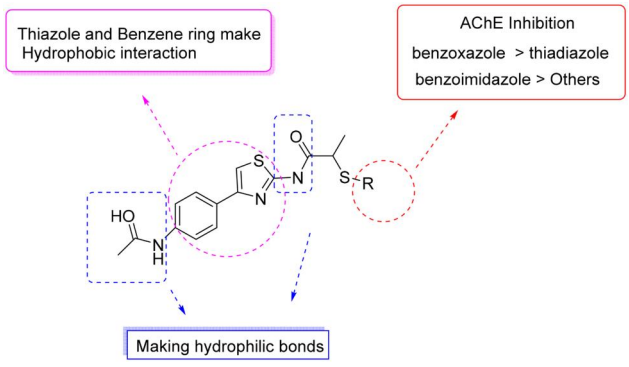

Figure 3. The structure–activity relationship.

Table 5. Synopsis of the Binding Interactions.

	PAS				CAS				
	Ser293 H-bond	Ser293 π–π	Trp286 π–π	Tyr341 π–π	Trp86 π–π	His447 π–π	Tyr341 π–π	Phe338 π–π	Asp74 X-bond
5d	✓		✓	✓		✓		✓	
5e	✓				✓		✓		
5j	✓	✓	✓	✓	✓				✓

3.4.1. The molecular docking of compound 5d

The interaction between compound **5d** with the active region in AChE is illustrated in Figure 5 and Figure 6. Five bonds bind the compound **5d** in AChE, four of them are π–π stacking bonds and a hydrogen bond. Two of the π–π stacking interactions are located in the CAS region formed between the thiadiazole ring and Phe338 and His447. The other two π–π stacking interactions are located in the PAS region formed between the thiazole ring with Tyr341, and between Trp286 with the benzene ring. The *NH*-benzene of the compound formed a hydrogen bond with Ser293.

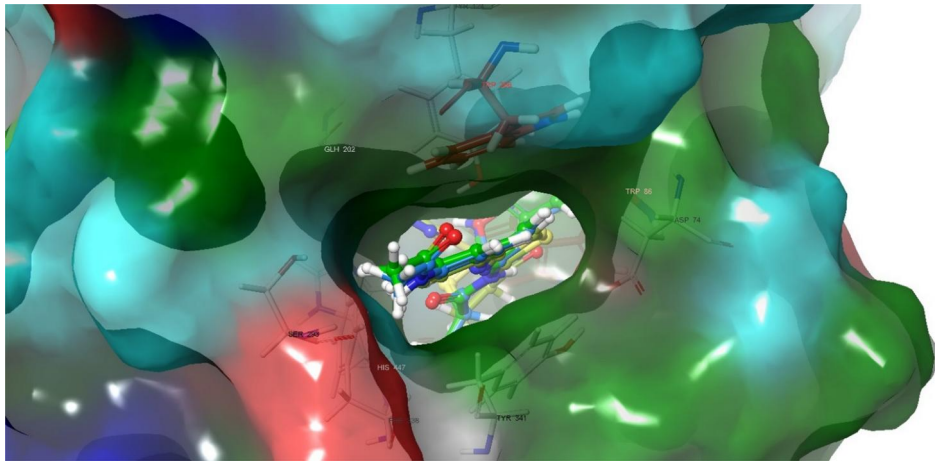

Figure 4. The three most active substances (**5d, 5e,** and **5j**) in the active site of AChE are layered in three dimensions.

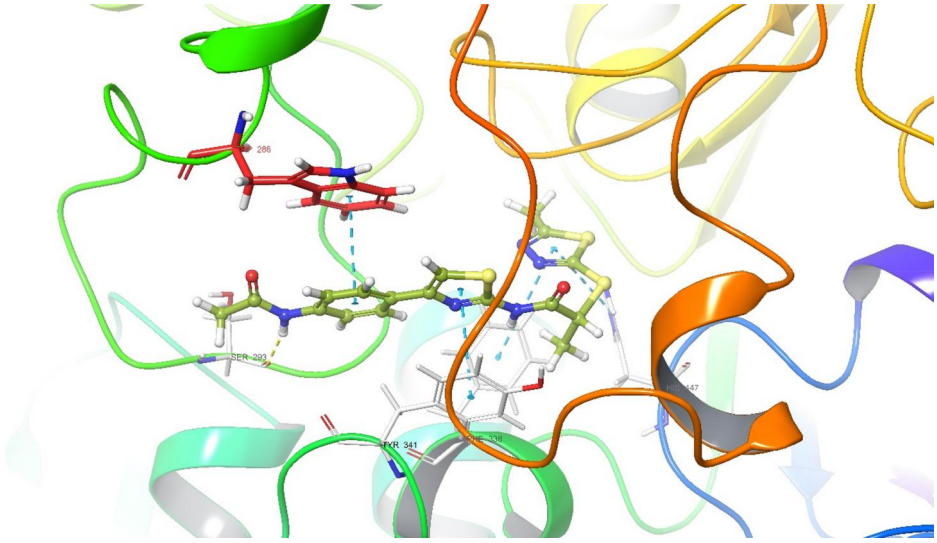

Figure 5. 3D interactions of compound **5d** at the (4EY7/PBDID) binding region of AChE.

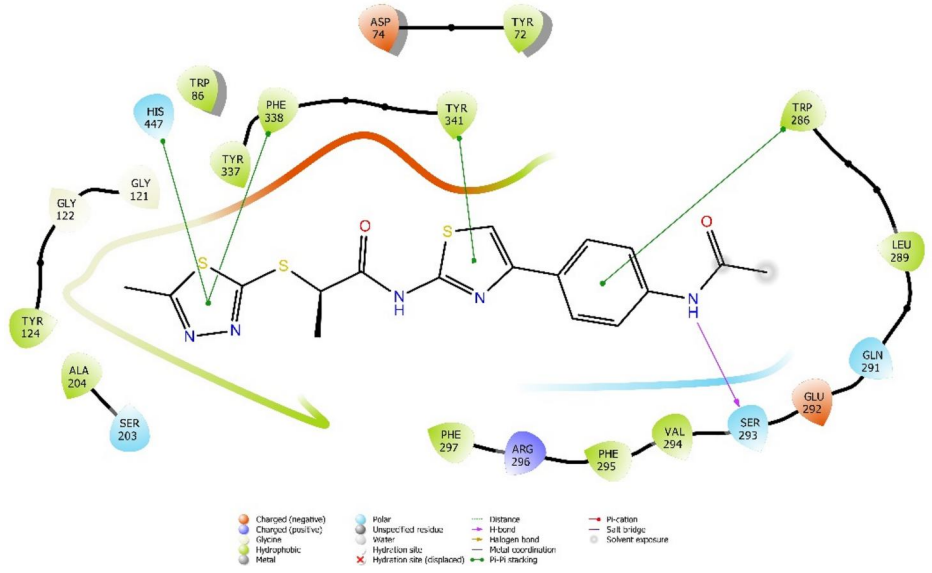

Figure 6. 2D interactions of compound **5d** at the (4EY7/PBDID) binding region of AChE.

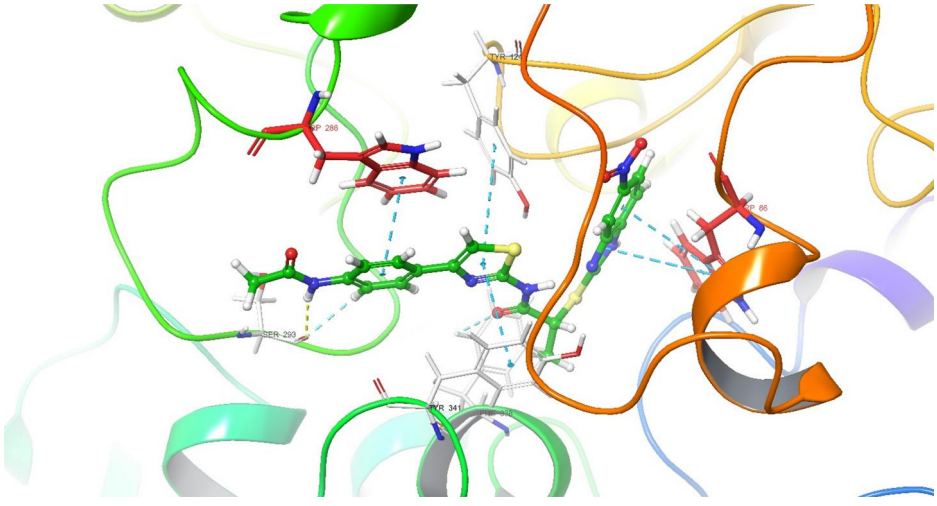

Figure 7. 3D interactions of compound **5e** at the (4EY7/PBDID) binding region of AChE.

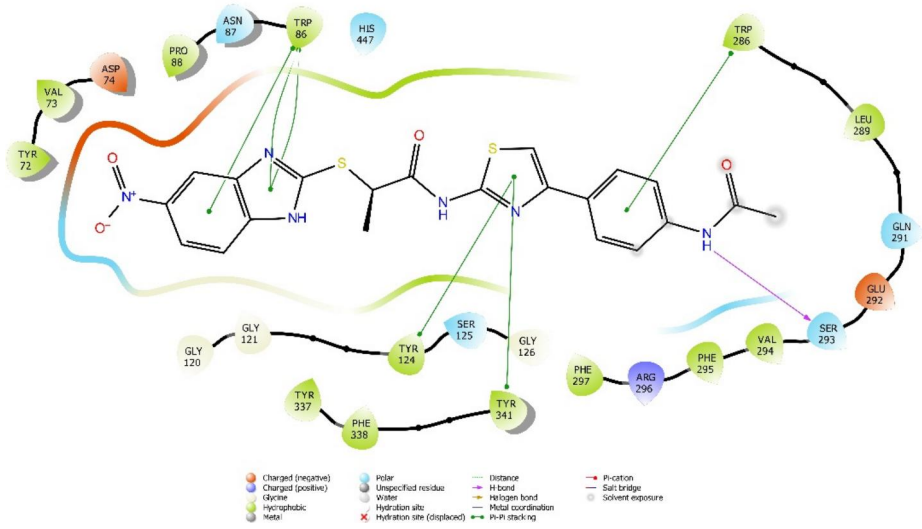

Figure 8. 2D interactions of compound **5e** at the (4EY7/PBDID) binding region of AChE.

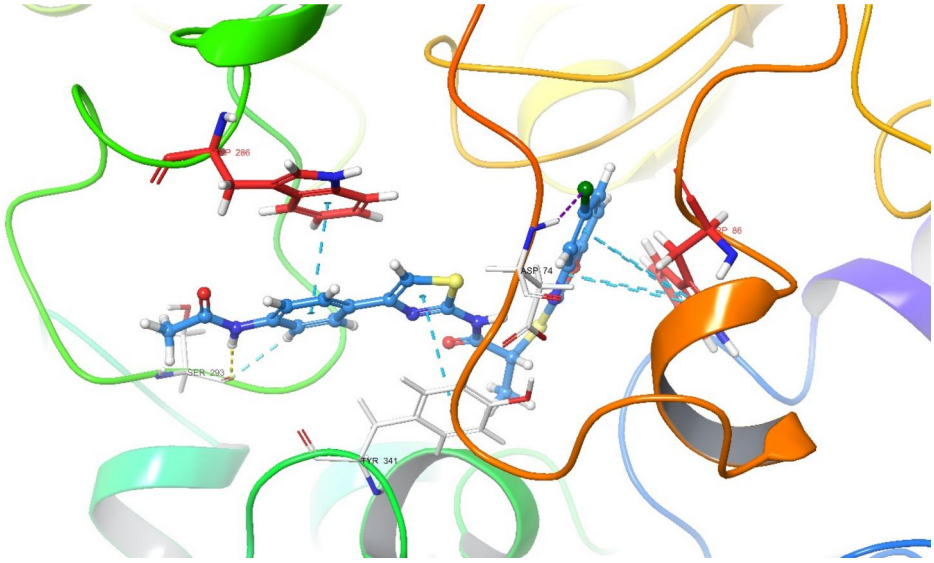

Figure 9. 3D interactions of compound **5j** at the (4EY7/PBDID) binding region of AChE.

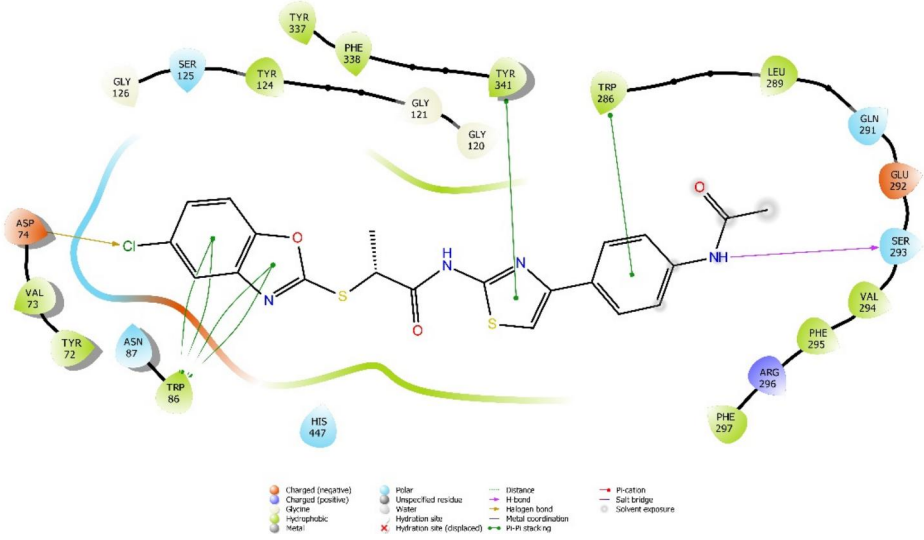

Figure 10. 2D interactions of compound **5j** at the (4EY7/PBDID) binding region of AChE.

3.4.2. The molecular docking of compound 5e

The following Figure 7 and Figure 8 (3D and 2D) illustrate the correlation between AChE and compound **5e** in seven bonds. Three of them between the benzothiazole ring and Trp86 bind by π–π stacking bonds in the CAS region. There are also three bonds linked by π–π stacking bonds tow between the thiazole ring with Trp124 and Tyr341, and one bond between the benzene ring and the Trp286 in the PAS region. In addition, in the PAS region, there is only one hydrogen bond between the NH-benzene and Ser293.

3.4.3. The molecular docking of compound 5j

The compound **5j** is the most active compound that has given effectiveness as an anti-acetylcholine esterase. The compound shows eight bonds, one of which is a halogenic bond between Asp74 and the chlorine atom that is connected to the oxathiazole ring. Also, four bonds formed between the oxathiazole ring and Trp86 by the π-π stacking bond in the CAS region. In the PAS region, there are also π–π stacking bonds one between the thiazole ring and Tyr341 and two bonds between the benzene ring with Trp286 and Ser 293 as shown in the 3D figure. Moreover, the last bond formed in the PAS region by a hydrogen bond between the NH-Benzene and Ser293. The following Figure 9 and Figure 10 illustrate the interconnection between the **5j** compound and the active site residues.

3.5. The MDS of compound 5j

The RMSD plot provides information on the stability and dynamics of the system being simulated. In general, a lower

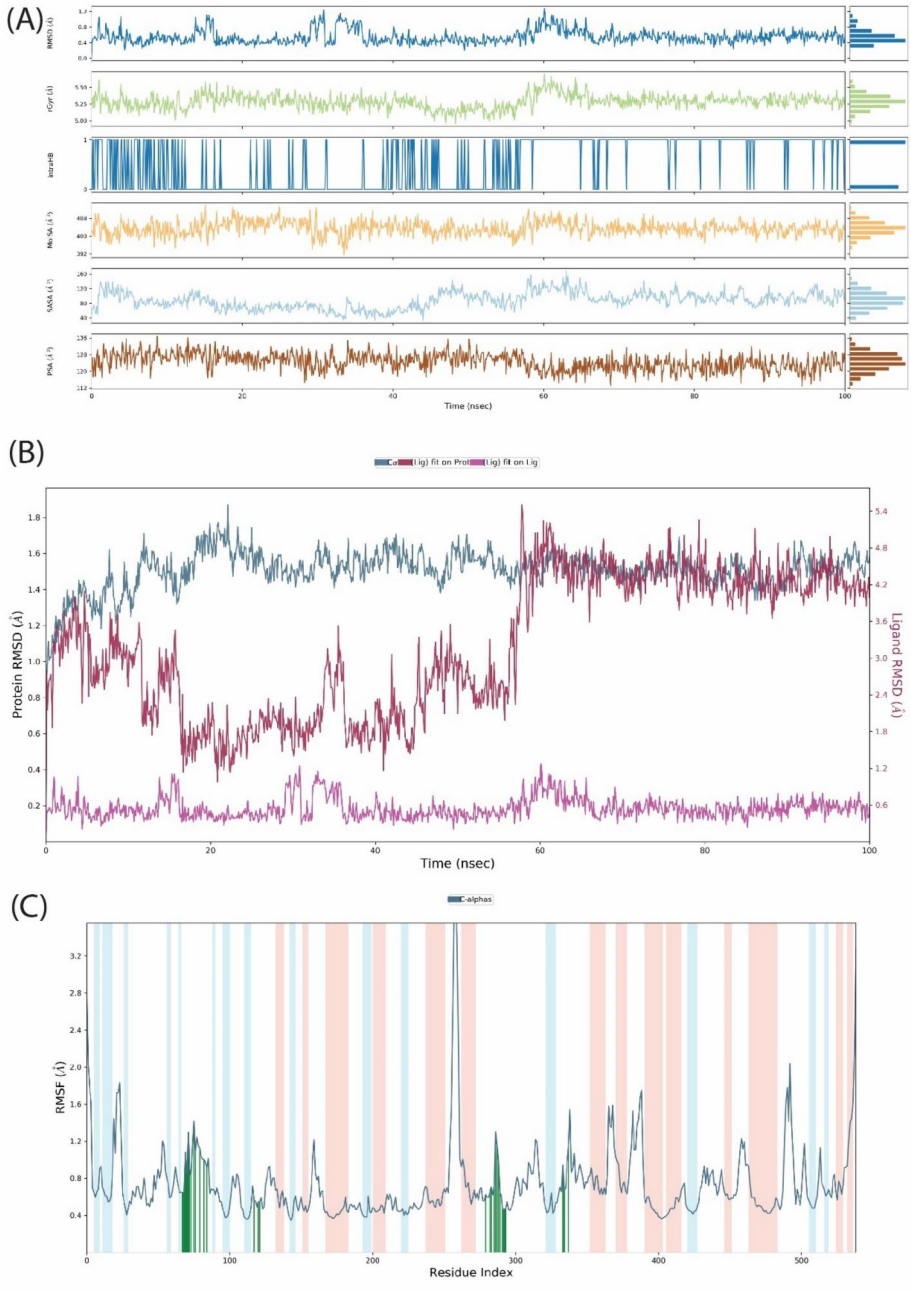

Figure 11. Molecular dynamic simulation (MDS) Results of **5j** ligand with AChE. (A) Rg, Plot. (B) Plot of root mean square deviation (RMSD) (Å)-time (ns). (C) Plot of root mean square fluctuation (RMSF)-residue index. The areas were represented in light red for the helices, light blue for the strands, and white for the loops.

RMSD value indicates that the system is more stable and closer to the starting structure, while a higher RMSD value indicates more structural deviation from the starting structure (Case et al., 2005; Lindorff-Larsen et al., 2010; Schweitzer-Stenner, 2014). The plot of RMSD value is 1.8 Å for protein and 1.2 Å. As Figure 11B, throughout the simulation, the protein–ligand system was found to be stable, as evidenced by the RMSD value of the protein falling within the range of 1–3 Å. Also, in radius of gyration (Rg), is a measure of the compactness of a protein–ligand complex. In MDS studies, Rg can be used to evaluate the quality of the predicted complex structure (Durrant et al., 2010). A lower fluctuation of Rg peaks (Figure 11A) indicates a more accurate prediction of the binding mode and a more stable complex.

The RMSF values measure the deviation of atomic positions in an MD simulation, providing insights into a molecule's flexibility and dynamics. High RMSF values indicate mobility and potential for interactions, while low RMSF values indicate rigidity. RMSF values can be plotted against residue numbers to identify flexible and rigid regions, aiding in the understanding of molecular behavior and interactions. The RMSF value was found to be low for α-helices (red areas) and β-strands (blue areas) in the protein complex, indicating that these regions were relatively rigid and did not experience higher than 1 Å during the simulation same as interacted loop regions. As Figure 11C the interaction between the ligand and enzyme was observed at less than 1 Å at the loop region and this observation provides evidence for a strong interaction between the ligand and protein.

The number of interactions by residue during a simulation is a measure of the frequency and strength of interactions between individual amino acid residues and other molecules.

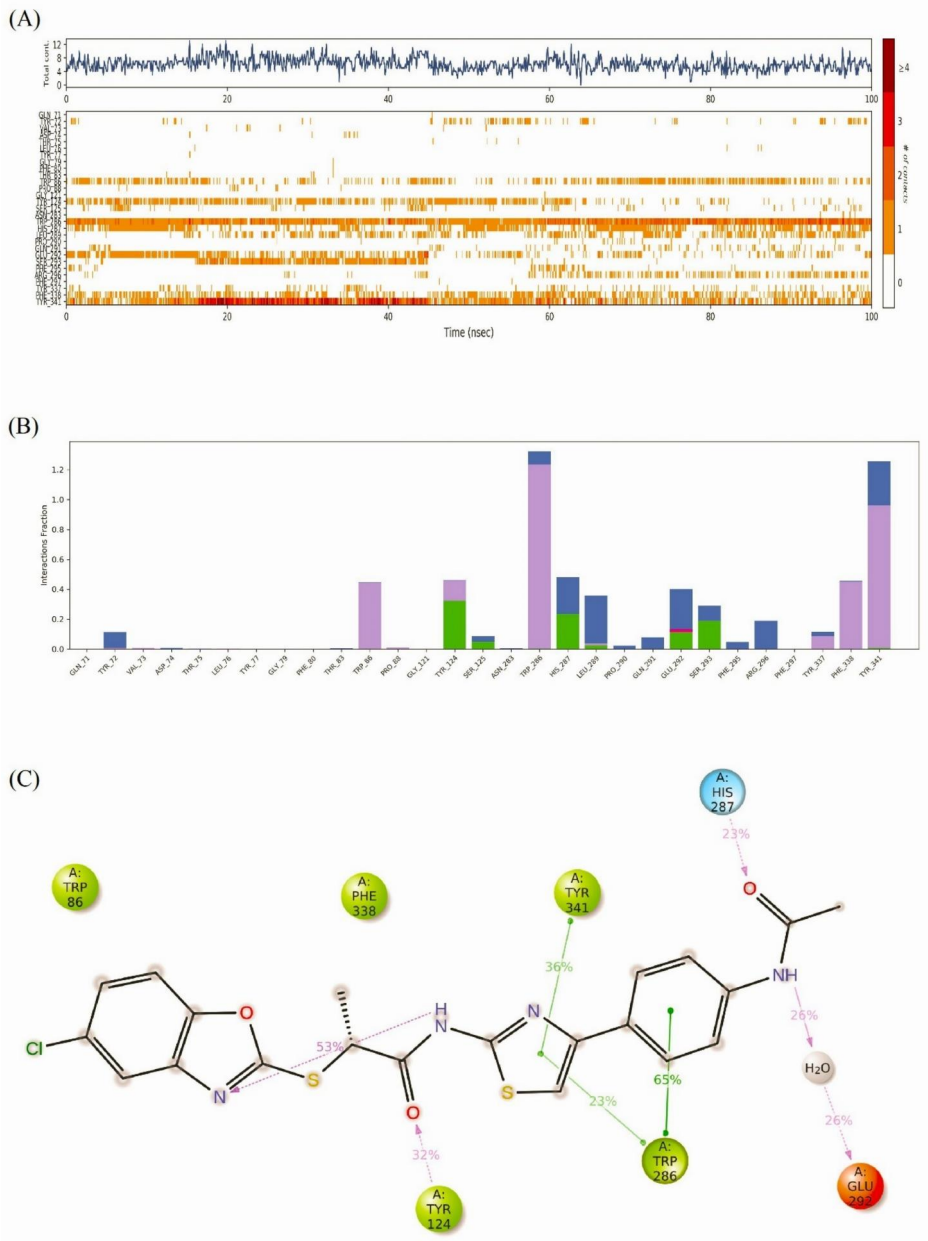

Figure 12. MDS Results of **5j** ligand with AChE (A) Number of interactions by residue during the simulation., (B) The plot of root means square fluctuation-residue index (blue: water-mediated H-bond; green, pink: ionic interaction, purple: hydrophobic interaction) (C) 2D diagram of the interaction strengths (cutoff = 20%).

It can provide insights into protein stability and identify key residues involved in specific interactions (Huang et al., 2017; Reddy et al., 2017). The docked pose compound **5j** reveals that amino acid residues such as Ser293 formed a hydrogen bond with the NH of the acetanilide moiety, whereas Trp86, Tyr341, and Trp286 formed π–π hydrophobic interactions with the aromatic rings with the phenyl, thiazole, and benzoxazole rings, respectively. In the 100 ns simulation, the hydrogen bond formed between the acetanilide NH and Ser293 did not sustain for more than 20% of the simulation time. Besides, in the first 20 ns, the acetanilide NH formed a new hydrogen/water-bridged hydrogen bond with Glu292 (Figure 12A). This interaction continued for more than 40% of the simulation period (Figure 12B). Also, the carbonyl of acetanilide formed new hydrogen and water-bridged hydrogen bonds with His287 and maintained it for 40% of the time (Figure 12B, C). Although the interaction between the ligand and Tyr341 was sustained throughout the simulation period, the π–π interaction formed between the thiazole ring and Tyr341 was sustained for 36% of the time. In addition, Tyr341 formed water-bridged hydrogen that did not last for more than 20% of the simulation time. However, thiazole also formed another π–π interaction with Trp286 which lasted for 23% of the simulation time. Besides interacting with the thiazole ring, Trp 286 showed a continuous π–π interaction with the phenyl ring, making it continuously interact with compound **5j** throughout the simulation time. Furthermore, the amide adjacent to the thiazole ring formed a new hydrogen bond with Tyr124 which lasted for 32% of the simulation time (Figure 12A, B). The π-π interactions formed between Trp86 and benzoxazole rind were preserved for approximately half of the simulation period (Figure 12B). In addition, compound **5j** formed interactions with Tyr72, Leu289, Phe295, Gln291, and Pro290 which were less than 20% of the simulation time (Figure 12E). In addition to these interactions, **5j** formed aromatic H-bonds (with Tyr72, Val73, Thr83, Trp86, Gly121, Tyr124, Ser125, Trp286, Glu292, Phe295, Arg296, and Phe297) and halogen bonds (Asp74, Tyr77, Gly79, Phe80, and Thr83) as seen in video. These findings indicated that the 5-chlorobenzoxazole ring is an appropriate structure since it is localized in the CAS pocket very well.

The key residues as described in previous studies (Al-Sharabi et al., 2023; Osmaniye et al., 2022; Sağlık et al., 2022). **5j** interacted with these key amino acids and also localized into the binding pocket of the AChE enzyme very well similar to donepezil. Thus, *in silico* studies revealed that the pivotal residues for this structure were identified as Trp86, Tyr124, Trp286, Tyr341, His287, and Glu292 residues. This finding clarified the binding mode between the acetylcholine esterase enzyme and **5j** and meanwhile, contributed to the structure-activity relationship. As a result, experimental findings were supported and clarified by *in silico* results, and they were in harmony.

4. Conclusions

The thiazole ring, a potential scaffold for developing drugs to treat neurodegenerative disorders like Alzheimer's and Parkinson's diseases, has been thoroughly investigated. In this study, a thiazole compound containing *N*-[4-(2-bromoacetyl)phenyl]acetamide was synthesized by reacting with thiourea under basic conditions. The compound was then acetylated, and mercapto-heterocyclic rings were added, resulting in a total of 12 compounds (**5a–5l**).

These synthesized compounds demonstrated increased effectiveness as AChE inhibitors. Specifically, compounds **5d, 5e,** and **5j** showed high inhibition efficiency against AChE with IC_{50} values of 0.223, 0.092, and 0.054 μM, respectively. However, all compounds exhibited low efficacy against BChE below 50% at concentrations of 10^{-3} and 10^{-4}, with significant IC_{50} values. Additionally, the MAO inhibitory activity of all compounds displayed weak inhibition percentages against both MAO-A and MAO-B, ranging from 20.415 to 38.461% at a concentration of 10^{-4}.

The three most effective compounds were subjected to docking analysis, which revealed strong associations with amino acids through hydrophilic, hydrophobic, hydrogen, and π–π stacking bonds. A detailed MDS study of compound **5j** found a halogen bond between the chlorine on the oxathiazole ring and Asp74, as well as four π–π stacking bonds between the oxathiazole ring and Trp86 in the CAS region. In the PAS region, π–π stacking bonds included one between the thiazole ring and Tyr341 and two between the benzene ring and Trp286 and Ser293.

For future research, it is suggested to introduce atoms such as halogens and nitro groups to the heterocyclic rings. The presence of a chlorine atom and a nitro group in the fifth position of the benzoxazole and benzimidazole rings in compounds **5j** and **5e** showed increased activity compared to compounds **5i** and **5f**, which lack these groups. This indicates that adding atoms and groups to these rings enhances activity and ligand-protein binding, as assessed in the *in vitro* activity and docking study.

Disclosure statement

No potential conflict of interest was reported by the authors.

Funding

This study was supported by the Anadolu University Scientific Research Project, Eskisehir, Turkey (Project no. 2212S199).

ORCID

Asaf Evrim Evren http://orcid.org/0000-0002-8651-826X

References

Abbas, N., Zaib, S., Bakht, S. M., Ibrar, A., Khan, I., Batool, S., Saeed, A., & Iqbal, J. (2017). Symmetrical aryl linked bis-iminothiazolidinones as new chemical entities for the inhibition of monoamine oxidases: Synthesis, in vitro biological evaluation and molecular modelling analysis. *Bioorganic Chemistry*, *70*, 17–26. https://doi.org/10.1016/j.bioorg.2016.11.004

Al-Sharabi, A. A., Evren, A. E., Sağlık, B. N., & Yurttaş, L. (2023). Synthesis, characterization, molecular docking and molecular dynamics simulations of novel 2, 5-disubstituted-1, 3, 4-thiadiazole derivatives as potential cholinesterase/monoamine oxidase dual inhibitors for

Alzheimer's disease. *Journal of Biomolecular Structure and Dynamics*, 1–19.

Andreani, A., Rambaldi, M., Leoni, A., Locatelli, A., Bossa, R., Chiericozzi, M., Galatulas, I., & Salvatore, G. (1996). Synthesis and cardiotonic activity of imidazo[2,1-b]thiazoles bearing a lactam ring. *European Journal of Medicinal Chemistry*, *31*(5), 383–387. https://doi.org/10.1016/0223-5234(96)89164-1

Bourne, Y., Taylor, P., & Marchot, P. (1995). Acetylcholinesterase inhibition by fasciculin: Crystal structure of the complex. *Cell*, *83*(3), 503–512. https://doi.org/10.1016/0092-8674(95)90128-0

Case, D. A., Cheatham, I. I. I. T. E., Darden, T., Gohlke, H., Luo. R., Merz, Jr., K. M., Onufriev, A., Simmerling, C., Wang, B., & Woods, R. J. (2005). The Amber biomolecular simulation programs. *Journal of Computational Chemistry*, *26*(16), 1668–1688. https://doi.org/10.1002/jcc.20290

Çevik, U. A., Işık, A., Evren, A. E., Kapusız, Ö., Gül, Ü. D., Özkay, Y., & Kaplancıklı, Z. A. (2022). Synthesis of new benzimidazole derivatives containing 1,3,4-thiadiazole: Their in vitro antimicrobial, in silico molecular docking and molecular dynamic simulations studies. *SAR and QSAR in Environmental Research*, *33*(11), 899–914. https://doi.org/10.1080/1062936X.2022.2149620

Ceyhun, İ., Karaca, Ş., Osmaniye, D., Sağlık, B. N., Levent, S., Özkay, Y., & Kaplancıklı, Z. A. (2022). Design and synthesis of novel chalcone derivatives and evaluation of their inhibitory activities against acetylcholinesterase. *Archiv der Pharmazie*, *355*(3), e2100372. https://doi.org/10.1002/ardp.202100372

Cummings, J. L. (2004). Alzheimer's disease. *The New England Journal of Medicine*, *351*(1), 56–67. https://doi.org/10.1056/NEJMra040223

Daina, A., Michielin, O., & Zoete, V. (2017). SwissADME: A free web tool to evaluate pharmacokinetics, drug-likeness and medicinal chemistry friendliness of small molecules. *Scientific Reports*, *7*(1), 42717. https://doi.org/10.1038/srep42717

Daoud, S., & Taha, M. O. (2020). Pharmacophore modeling of JAK1: A target infested with activity-cliffs. *Journal of Molecular Graphics & Modelling*, *99*, 107615. https://doi.org/10.1016/j.jmgm.2020.107615

Durmaz, Ş., Evren, A. E., Sağlık, B. N., Yurttaş, L., & Tay, N. F. (2022). Synthesis, anticholinesterase activity, molecular docking, and molecular dynamic simulation studies of 1, 3, 4 - oxadiazole derivatives. *Archiv der Pharmazie*, *355*(11), e2200294. https://doi.org/10.1002/ardp.202200294

Durrant, J. D., Amaro, R. E., Xie, L., Urbaniak, M. D., Ferguson, M. A. J., Haapalainen, A., Chen, Z., Di Guilmi, A. M., Wunder, F., Bourne, P. E., & McCammon, J. A. (2010). A multidimensional strategy to detect polypharmacological targets in the absence of structural and sequence homology. *PLoS Computational Biology*, *6*(1), e1000648. https://doi.org/10.1371/journal.pcbi.1000648

Evren, A. E., Karaduman, A. B., Sag, N., Yusuf, O., & Yurttas, L. (2023). Investigation of novel quinoline – thiazole derivatives as antimicrobial agents: In vitro and in silico approaches. *ACS Omega 8*(1), 1410–1429. https://doi.org/10.1021/acsomega.2c06871

Evren, A. E., Nuha, D., Dawbaa, S., Sağlık, B. N., & Yurttaş, L. (2022). Synthesis of novel thiazolyl hydrazone derivatives as potent dual monoamine oxidase-aromatase inhibitors. *European Journal of Medicinal Chemistry*, *229*, 114097. https://doi.org/10.1016/j.ejmech.2021.114097

Glish, G. L., & Vachet, R. W. (2003). The basics of mass spectrometry in the twenty-first century. *Nature Reviews. Drug Discovery*, *2*(2), 140–150. https://doi.org/10.1038/nrd1011

Greenblatt, H. M., Kryger, G., Lewis, T., Silman, I., & Sussman, J. L. Y. (1999). Structure of acetylcholinesterase complexed with (3) -galanthamine at î resolution. 2.3 A, 463321–463326.

Guo, J., O'Mahony, A. M., Cheng, W. P., & O'Driscoll, C. M. (2013). Amphiphilic polyallylamine based polymeric micelles for siRNA delivery to the gastrointestinal tract: In vitro investigations. *International Journal of Pharmaceutics*, *447*(1–2), 150–157. https://doi.org/10.1016/j.ijpharm.2013.02.050

Hardy, J., & Selkoe, D. J. (2002). The amyloid hypothesis of Alzheimer's disease: Progress and problems on the road to therapeutics. *Science (New York, N.Y.)*, *297*(5580), 353–356. https://doi.org/10.1126/science.1072994

Harel, M., Schalk, I., Ehret-Sabatier, L., Bouet, F., Goeldner, M., Hirth, C., Axelsen, P. H., Silman, I., & Sussman, J. L. (1993). Quaternary ligand binding to aromatic residues in the active-site gorge of acetylcholinesterase. *Proceedings of the National Academy of Sciences of the United States of America*, *90*(19), 9031–9035. https://doi.org/10.1073/pnas.90.19.9031

Heneka, M. T., Carson, M. J., El Khoury, J., Landreth, G. E., Brosseron, F., Feinstein, D. L., Jacobs, A. H., Wyss-Coray, T., Vitorica, J., Ransohoff, R. M., Herrup, K., Frautschy, S. A., Finsen, B., Brown, G. C., Verkhratsky, A., Yamanaka, K., Koistinaho, J., Latz, E., Halle, A., … Kummer, M. P. (2015). Neuroinflammation in Alzheimer's disease. *The Lancet. Neurology*, *14*(4), 388–405. https://doi.org/10.1016/S1474-4422(15)70016-5

Hirsch, E. C., & Hunot, S. (2009). Neuroinflammation in Parkinson's disease: A target for neuroprotection? *The Lancet. Neurology*, *8*(4), 382–397. https://doi.org/10.1016/S1474-4422(09)70062-6

Huang, J., Rauscher, S., Nawrocki, G., Ran, T., Feig, M., De Groot, B. L., Grubmüller, H., & MacKerell, A. D. Jr, (2017). CHARMM36m: An improved force field for folded and intrinsically disordered proteins. *Nature Methods*, *14*(1), 71–73. https://doi.org/10.1038/nmeth.4067

Huang, W., & Yang, G. F. (2006). Microwave-assisted, one-pot syntheses and fungicidal activity of polyfluorinated 2-benzylthiobenzothiazoles. *Bioorganic & Medicinal Chemistry*, *14*(24), 8280–8285. https://doi.org/10.1016/j.bmc.2006.09.016

Hussein, W., Sağlık, B. N., Levent, S., Korkut, B., Ilgın, S., Özkay, Y., & Kaplancıklı, Z. A. (2018). Synthesis and biological evaluation of new cholinesterase inhibitors for Alzheimer's disease. *Molecules (Basel, Switzerland)*, *23*(8), 2033. https://doi.org/10.3390/molecules23082033

Iqbal, K., Liu, F., & Gong, C.-X. (2016). Tau and neurodegenerative disease: The story so far. *Nature Reviews. Neurology*, *12*(1), 15–27. https://doi.org/10.1038/nrneurol.2015.225

Jankovic, J. (2008). Parkinson's disease: Clinical features and diagnosis. *Journal of Neurology, Neurosurgery, and Psychiatry*, *79*(4), 368–376. https://doi.org/10.1136/jnnp.2007.131045

Kalia, L. V., & Lang, A. E. (2015). Parkinson's disease. *Lancet (London, England)*, *386*(9996), 896–912. https://doi.org/10.1016/S0140-6736(14)61393-3

Kenyon, K., Contente, S., Trackman, P. C., Tang, J., Kagan, H. M., & Friedman, R. M. (1991). Lysyl oxidase and rrg messenger RNA. *Science (New York, N.Y.)*, *253*(5021), 802–802. https://doi.org/10.1126/science.1678898

Khan, K. M., Irfan, M., Ashraf, M., Taha, M., Saad, S. M., Perveen, S., & Choudhary, M. I. (2015). Synthesis of phenyl thiazole hydrazones and their activity against glycation of proteins. *Medicinal Chemistry Research*, *24*(7), 3077–3085. https://doi.org/10.1007/s00044-015-1349-1

Kumar, Y., Green, R., Borysko, K. Z., Wise, D. S., Wotring, L. L., & Townsend, L. B. (1993). Synthesis of 2,4-disubstituted thiazoles and selenazoles as potential antitumor and antifilarial agents: 1. Methyl 4-(Isothiocyanatomethyl)thiazole-2-carbamates, -selenazole-2-carbamates, and related derivatives. *Journal of Medicinal Chemistry*, *36*(24), 3843–3848. https://doi.org/10.1021/jm00076a012

Leoni, A., Frosini, M., Locatelli, A., Micucci, M., Carotenuto, C., Durante, M., Cosconati, S., & Budriesi, R. (2019). 4-Imidazo[2,1-b]thiazole-1,4-DHPs and neuroprotection: Preliminary study in hits searching. *European Journal of Medicinal Chemistry*, *169*(16989), 89–102. https://doi.org/10.1016/j.ejmech.2019.02.075

Lindorff-Larsen, K., Piana, S., Palmo, K., Maragakis, P., Klepeis, J. L., Dror, R. O., & Shaw, D. E. (2010). Improved side-chain torsion potentials for the Amber ff99SB protein force field. *PROTEINS: Structure, Function, and Bioinformatics*, *78*(8), 1950–1958. https://doi.org/10.1002/prot.22711

Lokwani, D. K., Sarkate, A. P., Karnik, K. S., Nikalje, A. P. G., & Seijas, J. A. (2020). Structure-based site of metabolism (SOM) prediction of ligand for CYP3A4 enzyme: Comparison of Glide XP and Induced Fit Docking (IFD). *Molecules (Basel, Switzerland)*, *25*(7), 1622. https://doi.org/10.3390/molecules25071622

Luo, A.-L., Zhao, Y.-H., Zhao, G., Deng, L.-C., Liu, X.-W., Jing, Y.-P., Wang, G., Zhang, H.-T., Shi, J.-R., Cui, X.-Q., Chu, Y.-Q., Li, G.-P., Bai, Z.-R., Wu, Y., Cai, Y., Cao, S.-Y., Cao, Z.-H., Carlin, J. L., Chen, H.-Y., … Zuo, F. (2015). The first data release (DR1) of the LAMOST regular survey. *Research in Astronomy and Astrophysics*, *15*(8), 1095–1124. https://doi.org/10.1088/1674-4527/15/8/002

Martorana, A., Giacalone, V., Bonsignore, R., Pace, A., Gentile, C., Pibiri, I., Buscemi, S., Lauria, A., & Palumbo Piccionello, A. (2016). Heterocyclic scaffolds for the treatment of Alzheimer's disease. *Current Pharmaceutical Design*, *22*(26), 3971–3995. https://doi.org/10.2174/1381612822666160518141650

Maryam, A., Khalid, R. R., Siddiqi, A. R., & Ece, A. (2021). E-pharmacophore based virtual screening for identification of dual specific PDE5A and PDE3A inhibitors as potential leads against cardiovascular diseases. *Journal of Biomolecular Structure & Dynamics*, *39*(7), 2302–2317. https://doi.org/10.1080/07391102.2020.1748718

Mc.Conathy, J., & Owens, M. J. (2003). Stereochemistry in drug action. *Primary Care Companion to the Journal of Clinical Psychiatry*, *05*(02), 70–73.

McKeith, I. G., Boeve, B. F., Dickson, D. W., Halliday, G., Taylor, J.-P., Weintraub, D., Aarsland, D., Galvin, J., Attems, J., Ballard, C. G., Bayston, A., Beach, T. G., Blanc, F., Bohnen, N., Bonanni, L., Bras, J., Brundin, P., Burn, D., Chen-Plotkin, A., … Kosaka, K. (2017). Diagnosis and management of dementia with Lewy bodies: Fourth consensus report of the DLB Consortium. *Neurology*, *89*(1), 88–100. https://doi.org/10.1212/WNL.0000000000004058

Meng, C., Zhang, J. C., Shi, R. L., Zhang, S. H., & Yuan, S. Y. (2015). Inhibition of interleukin-6 abolishes the promoting effects of pair housing on post-stroke neurogenesis. *Neuroscience*, *307*(307160), 160–170. https://doi.org/10.1016/j.neuroscience.2015.08.055

Millard, C. B., Kryger, G., Ordentlich, A., Greenblatt, H. M., Harel, M., Raves, M. L., Segall, Y., Barak, D., Shafferman, A., Silman, I., & Sussman, J. L. (1999). Crystal structures of aged phosphonylated acetylcholinesterase: Nerve agent reaction products at the atomic level. *Biochemistry*, *38*(22), 7032–7039. https://doi.org/10.1021/bi982678l

Hegab, M., Yousef, N., Nour, H., Ellithey, M., & Arbid, M. (2008). Synthesis and pharmacological activities of some condensed 4-chloro-2, 2-dialkyl chromene-3-carbaldehyde derivatives. *Acta Pharmaceutica*, *58*(1), 15–27.

Osmaniye, D., Evren, A. E., Karaca, Ş., Özkay, Y., & Kaplancıklı, Z. A. (2023). Novel thiadiazol derivatives; design, synthesis, biological activity, molecular docking and molecular dynamics. *Journal of Molecular Structure*, *1272*, 134171. https://doi.org/10.1016/j.molstruc.2022.134171

Osmaniye, D., Evren, A. E., Sağlık, B. N., Levent, S., Özkay, Y., & Kaplancıklı, Z. A. (2022). Design, synthesis, biological activity, molecular docking, and molecular dynamics of novel benzimidazole derivatives as potential AChE/MAO-B dual inhibitors. *Archiv der Pharmazie*, *355*(3), e2100450. https://doi.org/10.1002/ardp.202100450

Pålhagen, S., Heinonen, E., Hägglund, J., Kaugesaar, T., Mäki-Ikola, O., & Palm, R. (2006). Selegiline slows the progression of the symptoms of Parkinson disease. *Neurology*, *66*(8), 1200–1206. https://doi.org/10.1212/01.wnl.0000204007.46190.54

Prince, M. J., Wimo, A., Guerchet, M. M., Ali, G. C., Wu, Y.-T., & Prina, M. (2015). *The Global Impact of Dementia: An analysis of prevalence, incidence, cost and trends [Research Report]*. Alzheimer's Disease International ⟨hal-03495438⟩.

Reddy, R. H., Kim, H., Cha, S., Lee, B., & Kim, Y. J. (2017). Structure-based virtual screening of protein tyrosine phosphatase inhibitors: Significance, challenges, and solutions. *Journal of Microbiology and Biotechnology*, *27*(5), 878–895. https://doi.org/10.4014/jmb.1701.01079

Sağlık, B. N., Ilgın, S., & Özkay, Y. (2016). Synthesis of new donepezil analogues and investigation of their effects on cholinesterase enzymes. *European Journal of Medicinal Chemistry*, *124*(1241026), 1026–1040. https://doi.org/10.1016/j.ejmech.2016.10.042

Sağlık, B. N., Kaya Çavuşoğlu, B., Osmaniye, D., Levent, S., Acar Çevik, U., Ilgın, S., Özkay, Y., Kaplancıklı, Z. A., & Öztürk, Y. (2019). In vitro and in silico evaluation of new thiazole compounds as monoamine oxidase inhibitors. *Bioorganic Chemistry*, *85*, 97–108. https://doi.org/10.1016/j.bioorg.2018.12.019

Sağlık, B. N., Levent, S., Osmaniye, D., Evren, A. E., Karaduman, A. B., Özkay, Y., & Kaplancıklı, Z. A. (2022). Design, synthesis, and in vitro and in silico approaches of novel indanone derivatives as multifunctional anti-Alzheimer agents. *ACS Omega*, *7*(50), 47378–47404. https://doi.org/10.1021/acsomega.2c06906

Schapira, A. H. V., Chaudhuri, K. R., & Jenner, P. (2017). Non-motor features of Parkinson disease. *Nature Reviews. Neuroscience*, *18*(7), 435–450. https://doi.org/10.1038/nrn.2017.62

Schweitzer-Stenner, R. (2014). Cytochrome c: A multifunctional protein combining conformational rigidity with flexibility. *New Journal of Science*, *2014*, 1–28. https://doi.org/10.1155/2014/484538

Shintani, Y., Takashima, S., Asano, Y., Kato, H., Liao, Y., Yamazaki, S., Tsukamoto, O., Seguchi, O., Yamamoto, H., Fukushima, T., Sugahara, K., Kitakaze, M., & Hori, M. (2006). Glycosaminoglycan Modif. neuropilin-1 Modul. VEGFR2 signaling. *The EMBO Journal*, *25*(13), 3045–3055. https://doi.org/10.1038/sj.emboj.7601188

Siezen, R. J., & Galardini, M. (2008). Genomics of biological wastewater treatment. *Microbial Biotechnology*, *1*(5), 333–340. https://doi.org/10.1111/j.1751-7915.2008.00059.x

Spires-Jones, T. L., & Hyman, B. T. (2014). The intersection of amyloid beta and tau at synapses in Alzheimer's disease. *Neuron*, *82*(4), 756–771. https://doi.org/10.1016/j.neuron.2014.05.004

Tok, F., Koçyiğit-Kaymakçıoğlu, B., Sağlık, B. N., Levent, S., Özkay, Y., & Kaplancıklı, Z. A. (2019). Synthesis and biological evaluation of new pyrazolone Schiff bases as monoamine oxidase and cholinesterase inhibitors. *Bioorganic Chemistry*, *84*(8441), 41–50. https://doi.org/10.1016/j.bioorg.2018.11.016

Trawally, M., Demir-Yazıcı, K., Angeli, A., Kaya, K., Akdemir, A., Supuran, C. T., & Güzel-Akdemir, Ö. (2024). Thiosemicarbazone-benzene sulfonamide derivatives as human carbonic anhydrases inhibitors: synthesis, characterization, and in silico studies. *Anti-Cancer Agents in Medicinal Chemistry*, *24*(9), 649–667. https://doi.org/10.2174/0118715206290722240125112447

Trawally, M., Demir-Yazıcı, K., Dingiş-Birgül, S. İ., Kaya, K., Akdemir, A., & Güzel-Akdemir, Ö. (2022). Mandelic acid-based spirothiazolidinones targeting M. tuberculosis: Synthesis, in vitro and in silico investigations. *Bioorganic Chemistry*, *121*(January), 105688. https://doi.org/10.1016/j.bioorg.2022.105688

Tripathy, D., & Grammas, P. (2009). Acetaminophen inhibits neuronal inflammation and protects neurons from oxidative stress. *Journal of Neuroinflammation*, *6*(1), 10. https://doi.org/10.1186/1742-2094-6-10

Turan Yücel, N., Evren, A. E., Kandemir, Ü., & Can, Ö. D. (2022). Antidepressant-like effect of tofisopam in mice: A behavioural, molecular docking and MD simulation study. *Journal of Psychopharmacology (Oxford, England)*, *36*(7), 819–835. https://doi.org/10.1177/02698811221095528

Turan-Zitouni, G., Ozdemir, A., Kaplancikli, Z. A., Altintop, M. D., Temel, H. E., & Çiftçi, G. A. (2013). Synthesis and biological evaluation of some thiazole derivatives as new cholinesterase inhibitors. *Journal of Enzyme Inhibition and Medicinal Chemistry*, *28*(3), 509–514. https://doi.org/10.3109/14756366.2011.653355

Wang, W., Wang, D., Wang, Z., Yao, G., Li, X., Gao, P., Li, L., Zhang, Y., Wang, S., & Song, S. (2017). Synthesis of new sarsasapogenin derivatives with cytotoxicity and apoptosis-inducing activities in human breast cancer MCF-7 cells. *European Journal of Medicinal Chemistry*, *127*(12762), 62–71. https://doi.org/10.1016/j.ejmech.2016.12.011

Wang, Q., Zhao, Y., Chen, X., & Hong, A. (2022). Virtual screening of approved clinic drugs with main protease (3CLpro) reveals potential inhibitory effects on SARS-CoV-2. *Journal of Biomolecular Structure & Dynamics*, *40*(2), 685–695. https://doi.org/10.1080/07391102.2020.1817786

Yamali, C., Engin, F. S., Bilginer, S., Tugrak, M., Ozmen Ozgun, D., Ozli, G., Levent, S., Saglik, B. N., Ozkay, Y., & Gul, H. I. (2021). Phenothiazine-based chalcones as potential dual-target inhibitors toward cholinesterases (AChE, BuChE) and monoamine oxidases (MAO-A, MAO-B). *Journal of Heterocyclic Chemistry*, *58*(1), 161–171. https://doi.org/10.1002/jhet.4156

Yücel, N. T., Asfour, A. A. R., Evren, A. E., Yazıcı, C., Kandemir, Ü., Özkay, Ü. D., Can, Ö. D., & Yurttaş, L. (2024). Design and synthesis of novel dithiazole carboxylic acid Derivatives: In vivo and in silico investigation of their Anti-Inflammatory and analgesic effects. *Bioorganic Chemistry*, *144*, 107120. https://doi.org/10.1016/j.bioorg.2024.107120

Yücel, N. T., Osmaniye, D., Kandemir, Ü., Evren, A. E., Can, Ö. D., & Demir Özkay, Ü. (2021). Synthesis and antinociceptive effect of some thiazole-piperazine derivatives: Involvement of opioidergic system in the activity. *Molecules (Basel, Switzerland)*, *26*(11), 3350. https://doi.org/10.3390/molecules26113350

Zhao, G., Tong, Y., Luan, F., Zhu, W., Zhan, C., Qin, T., An, W., & Zeng, N. (2022). Alpinetin: A review of its pharmacology and pharmacokinetics. *Frontiers in Pharmacology*, *13*, 814370. https://doi.org/10.3389/fphar.2022.814370